Reduction of Unsteady Rotor-Stator Interaction Using Trailing Edge Blowing

by

Thomas A. Leitch

Thesis submitted to the Faculty of the
Virginia Polytechnic Institute and State University
in partial fulfillment of the requirements for the degree of

Master of Science

in

Mechanical Engineering

W.F. Ng, Chair

R.A. Burdisso

C.L. Dancey

January 16, 1997

Blacksburg, Virginia

Key words: Turbomachinery, Noise, Aeroacoustics, Trailing Edge Blowing

Reduction of Unsteady Rotor-Stator Interaction Using Trailing Edge Blowing

by

Thomas A. Leitch

Dr. W.F. Ng, Chairman

Mechanical Engineering

(ABSTRACT)

An aeroacoustic investigation was performed to assess the effects of adding mass flow at the trailing edges of four stators upstream of an aircraft engine simulator. By using trailing edge blowing to minimize the shed wakes of the stators, the flow into the rotor was made more uniform. In these experiments a reduced number of stators (four) was used in a 1/14 scale model inlet which was coupled to a 4.1 in (10.4 cm) turbofan engine simulator with 18 rotors and 26 downstream stators. This study is a preliminary step toward a more in depth investigation of using trailing edge blowing to reduce unsteady rotor-stator interaction. Steady-state measurements of the aerodynamic flow field and acoustic far field were made in order to evaluate the aeroacoustic performance at three simulator speeds: 40%, 60%, and 88% of the design speed. The lowest test speed of 40% design speed showed the most dramatic reduction in radiated noise. Noise reductions as large as 8.9 dB in the blade passing tone were recorded at 40% design speed, while a tone reduction of 5.5 dB was recorded at 60% design speed. At 88% design speed a maximum tone reduction of 2.6 dB was recorded. In addition, trailing edge blowing reduced the overall sound pressure level in every case. For both the 40% design speed and the 60% design speed, the fan face distortion was significantly reduced due to the trailing edge blowing. The addition of trailing edge blowing from the four upstream stators did not change the total pressure ratio, and the mass flow added by the blowing was approximately 1%. The results of these experiments clearly demonstrate that blowing from the trailing edges of the stators is effective in reducing unsteady rotor-stator interaction and the subsequent forward radiated noise.

Acknowledgments

I would like to thank W.F. Ng for providing me every opportunity to succeed. I would also like to thank R.A. Burdisso and C.L. Dancey for their insight and valuable time serving as advisory committee

I wish to extend a special thanks to Christopher Saunders, and Carol Steichen for their invaluable advice and tireless efforts in completing this work. I would also like to thank Randolph Hibshman, Kevin Miller, Todd Ninneman, Andy Nix, and David White. I truly value their friendship and company.

Most importantly, I would like to thank those closest to me, Lewis, Kathy, and Jennifer Leitch, and Katherine McArthur for their endless support.

Table of Contents

List of Illustrations

List of Tables

Nomenclature

dB	Decibel, sound pressure level, reference pressure 20×10^{-6} Pa
BPF	blade passing frequency
n	harmonic of BPF
B	number of rotors
N	shaft rotational speed (RPM)
r	radius
q	angular position (rad)
m	number of lobes or cycles of circumferential pressure variation
k	index
V	number of stators
Ω	shaft rotational speed (rad/sec)
Ω_m	mode rotational speed (rad/sec)
$k_{x\mathrm{m}}$	axial wave number
$k_{m\mathrm{m}}$	characteristic number associated with E-functions
k	wave number of standing wave
w	frequency (rad/sec)

c	speed of sound
σ	hub to tip ratio
m	radial nodes in the pressure patterns
f	frequency (Hz)
f_{mm}	cut-off frequency (Hz)
PNC	percent corrected fan speed
P_t	total pressure
SPL	sound pressure level

1.0 Introduction

The environmental impact of a jet aircraft engine has an important role in the overall design of a plane, and a major aspect of that environmental impact is the airport community noise. Densely populated areas are frequently exposed to excessive noise when engines are loudest and when aircraft are closest to the ground. The two most prominent sources of noise from jet engines are forward radiated fan noise and jet exhaust noise. Although jet exhaust noise is dominant during flight conditions, previous analysis by Trefny and Wasserbauer (1986) shows that "forward propagating fan noise is a significant noise component during takeoff and approach."

A primary generating mechanism of forward radiated noise is rotor-stator interaction. The three most common types of interactions are: rotor blades chopping through the wakes of upstream stators, wakes from rotor blades impinging on downstream stators, and the pressure fields of the rotors reflecting off nearby objects. The work in this thesis focuses on the first generating mechanism, where the rotor blades in the turbofan simulator cut through the wakes from four upstream stators in the inlet. As the blades rotate around, they periodically chop through these wakes and radiate noise. This study focuses on reducing the unsteady interaction between the stators and rotors by adding mass flow at the trailing edge of these upstream stators. The goal of trailing edge blowing from the stators is to make the flow going into the rotor more uniform. It is important to note that a zero-momentum wake is not necessarily a uniform wake. A zero-momentum wake could be highly non-uniform as long as the integral across the entire profile is zero.

This work is a preliminary step in the investigation of rotor-stator interaction and the subsequent radiated noise. In this experiment a reduced number of upstream stators was used. Only four stators, all with no turning angle and 0° angle of incidence, were placed upstream of the rotor. The results from this configuration will be used to focus a future study involving an increased stator count. The geometry of the inlet in this experiment is not entirely based on either subsonic or supersonic inlet design trends. The inlet is longer than a conventional subsonic inlet, but shorter than a supersonic inlet. It has a constant area profile and a simplified nose cone.

Based upon the inlet design, the results of this study have a number of applications in both subsonic and supersonic inlets.

The amount of published material regarding the aeroacoustic effects of wake management using trailing edge blowing is somewhat limited. Several experiments were performed to examine the effectiveness of different wake management strategies, and one experiment utilized results of wake management tests to make acoustic predictions. To the author's knowledge, this is the first published work to describe actual acoustic measurements resulting from wake management in a realistic turbomachinery environment.

Waitz, et al. (1995) predicted a significant acoustic benefit from blowing at the trailing edge of rotors in an aircraft engine. They predicted reductions in the strongest tonal harmonics of as much as 10 dB, in addition to reduction of the broadband noise. Their principal conclusion was that methods to control the fan wake are feasible for applications in high-bypass ratio turbomachines. However, this analytically-based conclusion was not substantiated by experimental data.

There has been considerable interest in studying how different mass addition configurations affect the resulting re-energized wakes. Using a variety of different mass addition methods, Park and Cimbala (1991), Corcoran (1992), and Naumann (1992) all demonstrated that trailing edge blowing from flat plates can significantly reduce time-mean wake deficits downstream. The different trailing edge configurations included single continuous slits, double continuous slits, single rows of discrete jets, double rows of discrete jets, and the addition of vortex generators.

This thesis is organized into five chapters. The next chapter describes previous research on trailing edge blowing and gives background information on the generation and propagation of fan noise. Chapter 3 details the test procedures, facilities, inlet design, blowing technique, and instrumentation. Chapter 4 provides the aerodynamic and acoustic comparisons of the blowing versus no blowing cases. Chapter 5 examines the experimental results from the Chapter 4 and draws a number of conclusions.

2.0 Background

This chapter consists of two sections. The first part describes previous research relevant to trailing edge blowing. The second section examines at the physics of noise generation and duct acoustics and how it relates to this research.

2.1 Previous Research in Trailing Edge Blowing

Park and Cimbala (1991), Corcoran (1992), and Naumann (1992) demonstrated that trailing edge blowing can significantly reduce time-mean wake deficits and unsteadiness downstream from a flat plate. Corcoran (1992) and Naumann (1992) experimented with several blowing techniques and configurations in a closed-circuit water channel. They both found that trailing edge blowing is effective in attenuating the mean wake deficit from the edge of a flat plate. In addition, Corcoran (1992) showed that trailing edge blowing reduces Reynolds stress, vorticity, and velocity fluctuations within one chord length downstream. They also noted that the fluid characteristics of re-energized wakes are highly dependent upon the method that was used to generate them.

Naumann (1992) examined several different configurations for trailing edge blowing, including a continuous slit at the trailing edge, a set of discrete jets, and a set of discrete jets with vortex generators. Naumann's work showed that of these configurations discrete jets provide the best results. Furthermore, he went on to show that vortex generators enhance downstream mixing of the trailing edge blowing air and the wake.

Waitz, et al. (1995) used trailing edge blowing along with boundary layer suction on an actual rotor blade in an effort to minimize the shed wake. This study used two-dimensional numerical and experimental models to determine how wake modification effects radiated noise. The magnitude of the radiated noise was estimated using LINSUB, a two-dimensional, linearized

panel method. Using the experimental and numerical wake profiles, LINSUB was then used to calculate the amplitudes of the radiated acoustic waves. These experiments were performed in a wind tunnel facility using a stationary rotor blade with a chord of 9.8 in (25 cm) and span of 11.8 in (30 cm). Trailing edge blowing was accomplished using 0.06 in (1.5 mm) internal diameter tubes center spaced at 0.12 in (3 mm).

Waitz, et al. (1995) concluded that wake management is feasible for high-bypass turbomachinery. Acoustic predictions based on the aerodynamic data suggest that the strongest tonal harmonics can be reduced by more than 10 dB. Trailing edge blowing reduced the time mean wake deficit by 50% and the turbulent velocity fluctuations by 45% at a downstream distance of 1.5 chord lengths. The amount of air added through the trailing edge blowing was less than 1% of the overall fan mass flow.

All of the works previously discussed were geared toward applying wake management to rotor-stator interaction. However, it is important to note that there is a separate noise generating mechanism at work, noise from the rotor only. A common example of this noise is that which is radiated from helicopter rotors and propeller-driven aircraft. Succi (1993) examined techniques to suppress the noise associated with the rotor only. By carefully applying blowing and suction strategies along the span of the rotor, he predicted that significant rotor noise attenuation was achievable. Waitz, et al. (1995) cited that many of the blowing and suction strategies designed to suppress noise from rotor-stator interaction could either increase or decrease the noise which is associated with the rotor only. However, they went on to conclude that for high-bypass turbofans any additional rotor noise resulting from wake management was small when compared with rotor-stator interaction noise.

2.2 Noise Generation, Transmission, and Radiation

In experimental work with compressors there are usually three types of noise considered: broadband noise, combination tone noise, and discrete tone noise. Broadband noise is relatively equally distributed among all of the frequencies in the spectrum. This broadband noise can be caused by vortex shedding, boundary layer turbulence, interaction of the blade pressure fields and inlet turbulence, and interaction between the blade pressure fields and wall boundary layers. Combination tones, otherwise known as multiple pure tones or “buzz-saw” tones, onset when the relative Mach number of the rotor blade tips exceeds unity. Because of the highly nonlinear nature of the leading edge shocks on each of the blades and small manufacturing discrepancies between the blades, there are deviations between the shock amplitudes and spacing. As a result, tones appear at integer multiples of the fan rotational frequency. For example, the simulator used in these experiments has 18 blades rotating at 70,000 RPM. The combination tones thus occur at 1167 Hz intervals.

Discrete tone noise has been the most widely studied aspect of compressor noise. This tone occurs at the blade passing frequency and its harmonics.

$$BPF\,(\text{Hz}) = \frac{nBN}{60}; \quad n = 1, 2, 3,... \tag{2.1}$$

where: n = harmonic of the blade passing frequency
B = number of rotor blades
N = shaft rotational speed (RPM)

Tyler and Sofrin (1961) examined discrete tone noise in compressors by decomposing the problem into three constituent parts: generating mechanisms, duct transmission, and radiation into the far field.

The rotor-stator interaction in a compressor produces a number of standing waves or modes. In the cylindrical geometry of a compressor and inlet, these standing waves exist in both the radial (r) direction and the circumferential (θ) direction. The circumferential modes have a very distinct number of lobes (amplitude peaks) in the pressure pattern given by

$$|m| = nB + kV, \qquad k = ...-1,0,1,... \tag{2.2}$$

where: n = harmonic index
B = number of rotor blades
k = index
V = number of stator blades

In other words, multiples of the number of vanes (kV) are added and subtracted from the product of the harmonic number multiplied by the number of rotor blades (nB). It is these lobes that produce the blade passing tone and its harmonics. Furthermore, these pressure patterns are not stationary. Depending on the number of lobes a pressure pattern has, it will rotate at a different speed in order to produce the blade passing frequency or an associated harmonic. The rotation speed of the mode is given by

$$\Omega_m = \frac{nB}{m}\Omega \tag{2.3}$$

where: m = number of lobes or cycles of circumferential pressure variation
n = harmonic index
B = number of rotors
Ω = shaft rotational speed (rad/sec)

Unless $m = B$, the lobed pressure pattern must rotate at a different speed than the shaft in order to produce the tone at the blade passing frequency. For one blade, a one-lobed ($m = 1$) standing wave pattern must rotate at the shaft speed in order for the lobe to pass at the same frequency as the blade. The same is true for an eight-lobed pattern ($m = 8$) with eight blades. However, if $m = 8$ and $B = 16$, there are only half as many lobes as blades and the standing wave must rotate at twice the shaft speed in order to produce the blade passing frequency. Similarly, the pattern must rotate at four times the shaft speed to produce the first harmonic of the blade passing frequency. For a particular harmonic of the blade passing frequency, the noise field is a superposition of an infinite number of these rotating patterns all rotating at different velocities.

Having considered the noise generating mechanism, one must now look at how the pressure waves propagate forward into the inlet. In fact, one must determine whether a given mode will propagate through the inlet at all. The axial wave number, k_{xm}, governs whether or not a pressure pattern will propagate down the axis of an inlet and is given by

$$k_{xm} = \sqrt{k^2 - k_{mm}^2}$$
$$k_{xm} = \frac{2\pi}{c}\sqrt{f^2 - f_{mm}^2} \qquad (2.4)$$

where: c = speed of sound

$k = \frac{\omega}{c}$ is the wave number for the standing wave

k_{mm} = characteristic number associated with the E-functions depending upon hub to tip ratio (σ), number of circumferential lobes (m), and the number of nodes or points of zero pressure across the annulus (n).

f = frequency of the standing wave

f_{mm} = cut-off frequency

The cut-off frequency is associated with the E-functions describing the radial pressure distribution, hub to tip ratio of the inlet, the number of circumferential lobes, and the number of nodes or zero pressure points across the annulus. E-functions are linear combinations of Bessel functions of the first and second kinds which emerge directly from the solution of the acoustic wave equation in cylindrical coordinates. If the frequency of interest, f, is less than the cut-off frequency, f_{mm}, then the axial wave number will be imaginary. An imaginary wave number means that the amplitude of the pressure waves will exponentially decay down the axis of the inlet, and these waves are termed evanescent waves. In the case of a real axial wave number, k_{mm}, the pressure pattern will propagate down the inlet and radiate to the far field.

Once the sound propagates to the end of the inlet, it is free to radiate into the far field. As the pressure waves propagate from the inlet into an infinite, homogeneous, and isotropic medium,

the boundary condition at infinity is that there is no reflection. The radiation pattern (directivity) in the far field can be relatively complex. It can be shown that only a plane wave (m = 0 mode) propagating from the duct has the peak of its far field pressure on the axis of the inlet. All other modes have a pressure of zero at this position. As the frequency increases the radiated field becomes more focused toward the centerline.

3.0 Experiment

This chapter describes the experimental setup. The first part describes the turbofan simulator. The second section illustrates the inlet geometry and blowing configuration, and the third section examines the test facility. Sections four and five describe the instrumentation and measurements (both aerodynamic and acoustic). Finally, section six details the test matrix for this experiment.

3.1 Turbofan Simulator

The noise source used in this experiment was a Tech Development Model 460 turbofan simulator. This model functions like a fan in a high bypass ratio engine. Figure 3.1 shows the simulator and its rotating components. The simulator is powered by high-pressure air exhausting through a single-stage turbine with 29 blades and a maximum mass flow of 1.50 lbm/sec (0.68 kg/sec). This turbine turns a single stage fan that draws air into the simulator from the ambient atmosphere. The two different air streams (high-pressure turbine air and ambient fan air) are then mixed downstream of the simulator exit.

With a diameter of 4.1 inches, the single-stage fan has 18 fan blades, 26 stator blades, and an exit area of 5.7 in^2. The Model 460 has a design speed of 80,000 RPM or 100 percent corrected fan speed (PNC), and is capable of producing a total pressure ratio of 1.6 with a mass flow of 2.72 lbm/sec (1.23 kg/sec). The instrumentation includes a magnetic pickup tachometer to measure the shaft rotational speed and thermocouples to monitor the bearing temperatures.

In this experiment, the simulator was tested at 30,000 RPM (40 PNC), 50,000 RPM (60 PNC), and 70,000 RPM (88 PNC). Simulated approach speed for the Model 460 is 50,000 RPM

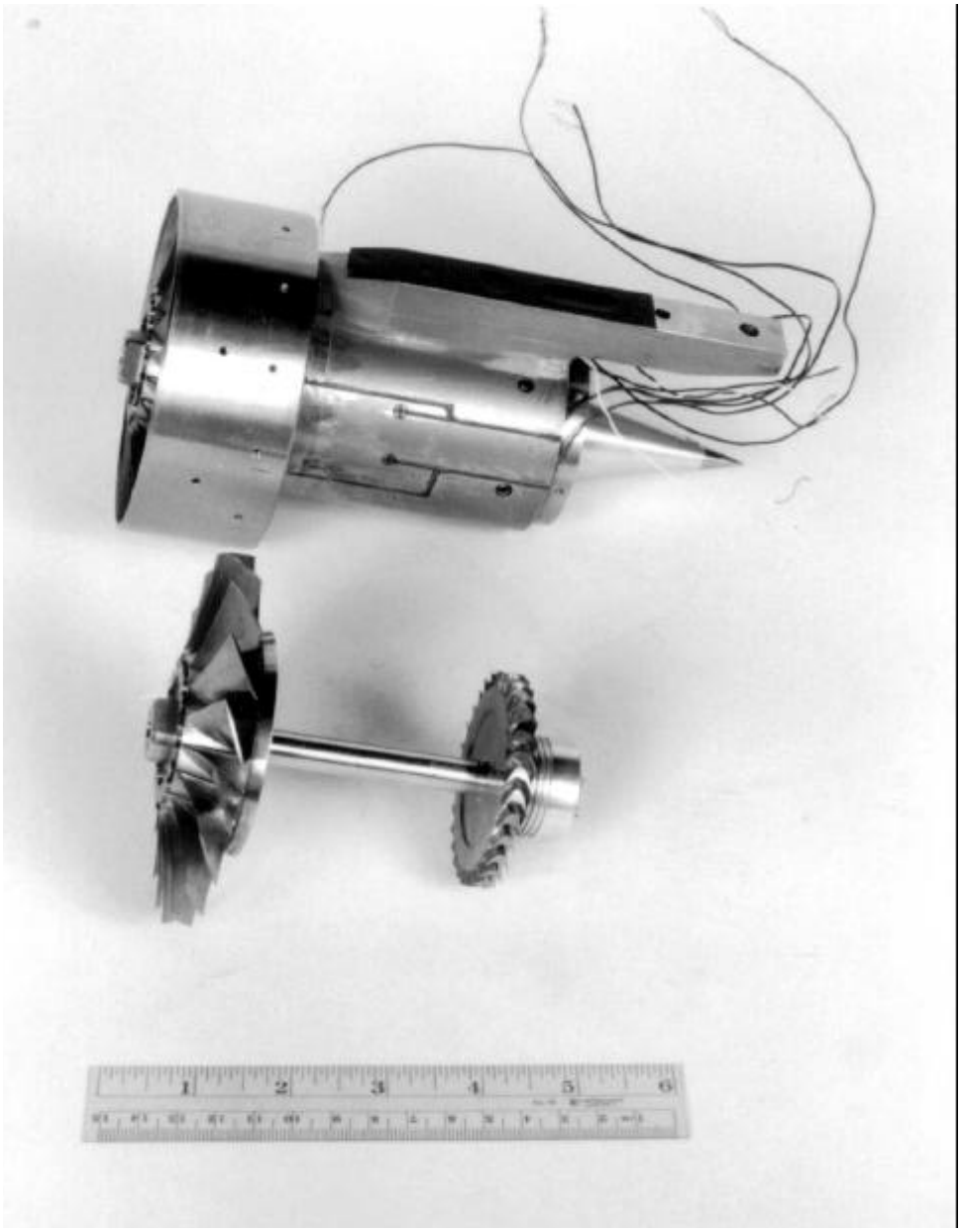

Figure 3.1 Turbofan Engine Simulator

(60 PNC), and the simulated takeoff speed is 70,000 RPM (88 PNC). At 65,000 RPM (80 PNC), the blade tip speed becomes supersonic, and combination tone noise onsets.

3.2 Blowing Stators

In this study, the turbofan simulator was coupled to the inlet shown in Figure 3.2. The challenge was to design a test inlet that would be flexible enough for the results to be applicable to a wide variety of inlets, while focusing on rotor-stator interaction and reducing or eliminating other factors that influence the acoustic results. The geometry of the inlet in this experiment is not entirely based on either subsonic or supersonic inlets. The inlet was designed so that the experimental results would be applicable to both subsonic and supersonic inlets. For example, the results of this experiment are of interest when examining rotor-stator interaction in all types of turbomachinery. However, these results can also be directly applied to rotor-strut interaction in supersonic inlets. This inlet is longer than a conventional subsonic inlet and is equipped with a centerbody supported by the stators. In order to reduce boundary layer effects, the inlet is shorter than a typical supersonic inlet. The centerbody is greatly simplified, and the outer profile is made so that the inlet has a constant area profile. The constant area profile does not accelerate the flow through the inlet. Miller (1995) noted that as the flow Mach number approaches 0.5, a soft choking effect lowers the tone and overall sound pressure levels radiated into the far field. Figure 3.3 compares the inlet used in this study and a representative supersonic and subsonic inlets.

The bellmouth on the inlet helps prevent boundary layer separation at the cowl surface during the static tests. The bellmouth is identical to those used in previous experiments. Miller (1995) observed large regions of flow separation originating from a sharp cowl lip. The addition of a bellmouth to the inlet prevented the onset of boundary layer separation.

Each of the stators in the inlet has a chord length of 2.25 in (5.72 cm) with a span of 1.25 in (3.18 cm). The stators have no turning angle and have a 0° incidence angle. The stators are positioned so that the fan face is 75% of the chord length downstream from the trailing edges. This axial distance between the stators and fan face provided the wake with an opportunity to mix with the trailing edge blowing air before they impinge upon the rotating fan blades.

The most important aspect of the stator design is the configuration of the holes at the trailing edge. Trailing edge blowing is accomplished using six holes, equally-spaced at 0.17 in (4.3 mm). The blowing air is fed to these six holes by a 0.125 in (3.2 mm) diameter circular passage. The diameters of the holes from tip to hub are: 0.063 in (1.6 mm), 0.063 in (1.6 mm), 0.063 in (1.6 mm), 0.047 (1.2 mm), 0.032 in (0.8 mm), and 0.032 in (0.8 mm). The blowing air

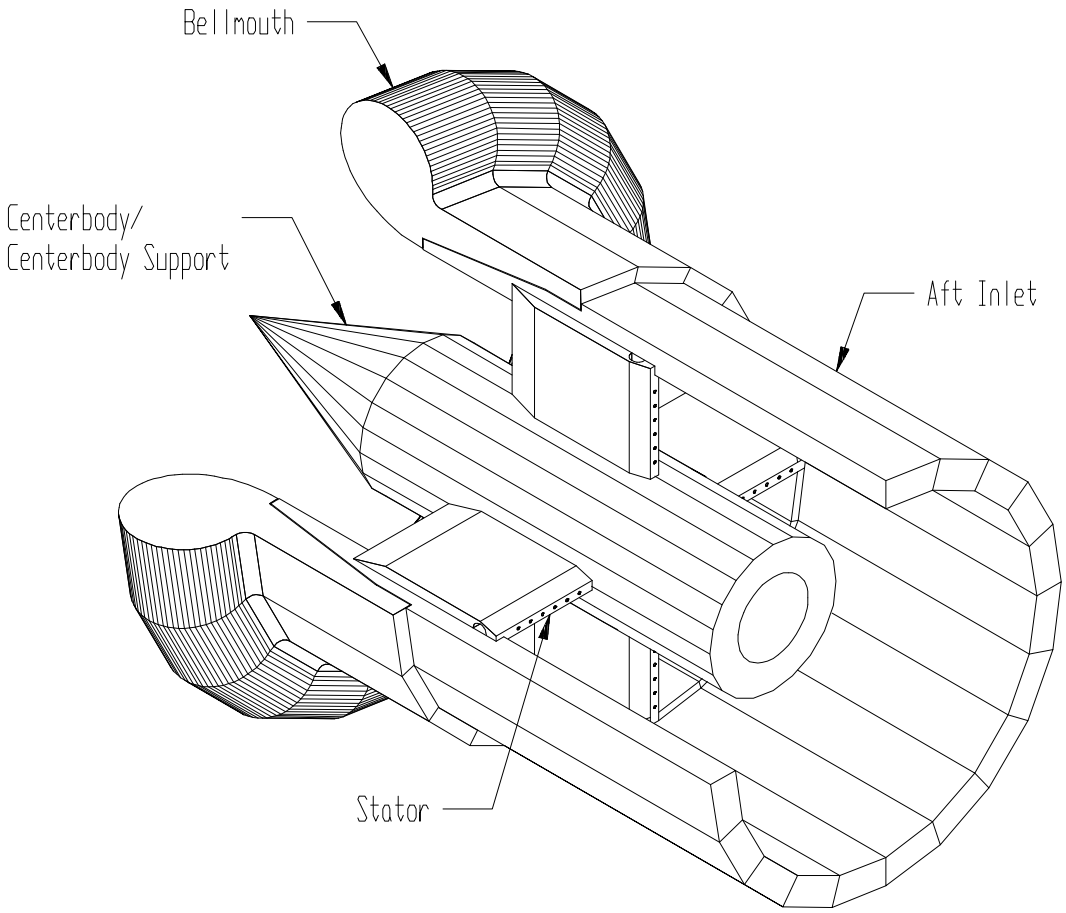

Figure 3.2 Cutaway View of the Virginia Tech Inlet

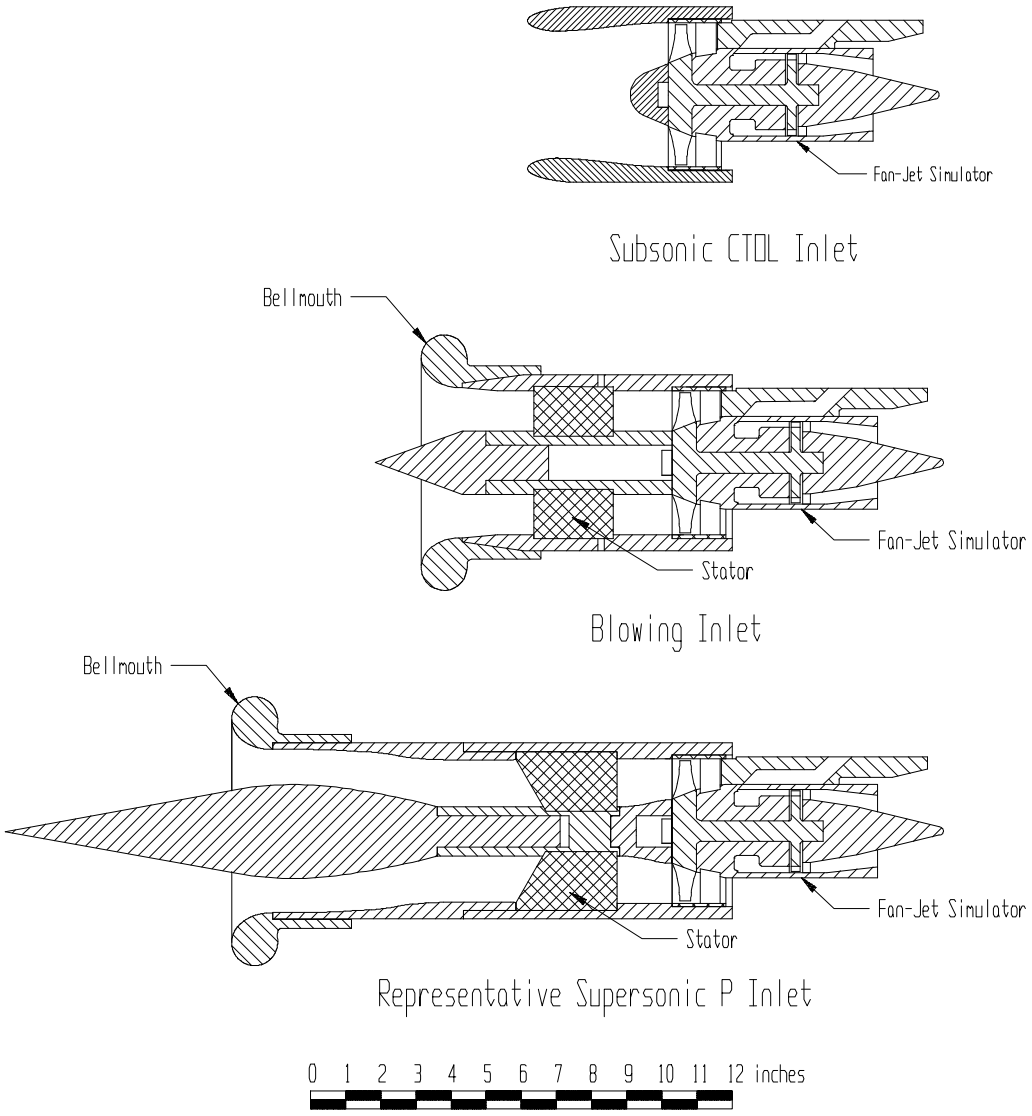

Figure 3.3 The Virginia Tech Inlet Compared to Supersonic and Subsonic Inlets

is supplied to this circular passage from outside the inlet, and each of the six smaller holes taps off of the circular passage. Figure 3.4 illustrates how the blowing air supply lines mate with the inlet and stators on the test stand. In order to drill the six holes for the blowing air into each of the stators, the trailing edges had to be cut. Instead of tapering to a sharp edge, the trailing edges of each stator have a thickness of 0.0625 in (1.6 mm).

The goal in designing a trailing edge configuration was to produce a uniform blowing profile from the tip to the hub. A secondary consideration was that the hole configuration be designed to use a minimal amount of blowing air. In order to achieve the most uniform profile possible, a series of bench tests was initiated to help design the trailing edges of the stators. The main problem is that the only exit from the circular passage is through the trailing edge blowing holes. The flow reaches the bottom of the passage and stagnates, causing a rise in total pressure. Because of this non-uniform pressure profile inside the supply passage, it is difficult to achieve a uniform blowing profile at the trailing edge. If equally-spaced holes of the same diameter are used, most of the blowing air exits through the bottom holes. The simplest solution to obtain a more uniform profile was to use larger trailing edge holes at the tip and smaller ones at the hub.

Two different hole configurations were investigated, six equally-spaced holes and nine equally-spaced holes. In order to determine the best hole sizes to use, all of the holes were drilled to the same diameter. Pieces of steel tubing with different inner diameters were then inserted into the holes. By replacing the tubing with pieces of different inner diameters, a variety of hole sizes could be tested and compared.

After extensive testing of different trailing edge configurations, it was found that six equally-spaced holes provided the best results in re-energizing the wake. Figure 3.5 details the stator geometry. Six discrete jets were effective in re-energizing the wake while adding a relatively small amount of air to the overall mass flow through the fan. Appendix A outlines the bench tests and presents the results. This bench test proved to be a crucial part of the experiment. Because the blowing configuration can dramatically affect the wake, it is important to design and test the trailing edge configuration based upon its intended application. It would be very difficult to scale the design of these stators to a different application and achieve similar results.

The source for the blowing air is a high-pressure air cylinder located outside the anechoic chamber. Air travels from this cylinder to a large cylindrical plenum near the inlet through 18 ft (5.49 m) of 0.25 in (6.35 mm) ID copper tubing. Next the air is piped from the plenum to each of the four stators through four pieces of 0.125 in (3.18 mm) ID copper tubing, each 1.875 ft (0.57 m) in length. The plenum has one inlet, four exits, a diameter of 4 in (10.2 cm), and a height of 41 in (104 cm). As with the air flow to the simulator, the flow rate of the blowing air to the stators is manually controlled using a hand valve. Figure 3.6 illustrates the equipment used to achieve the blowing on each of the four stators.

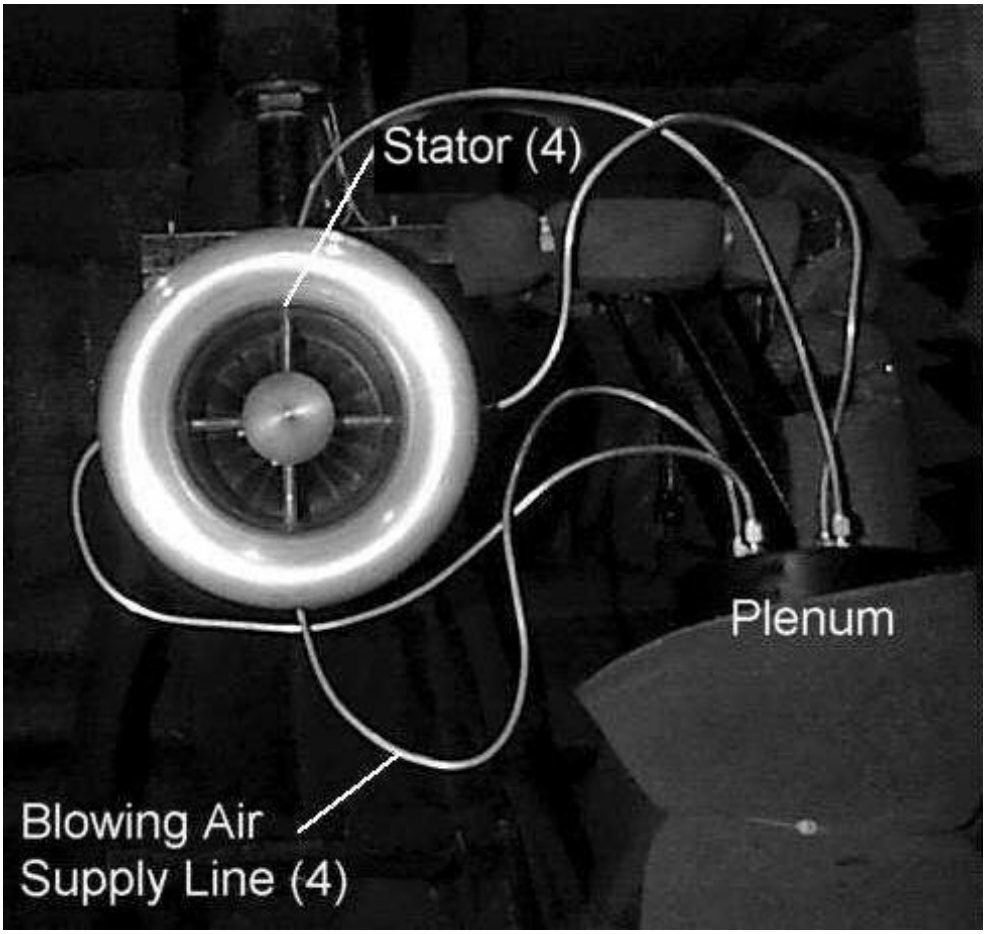

Figure 3.4 Blowing Air Supply Into Inlet

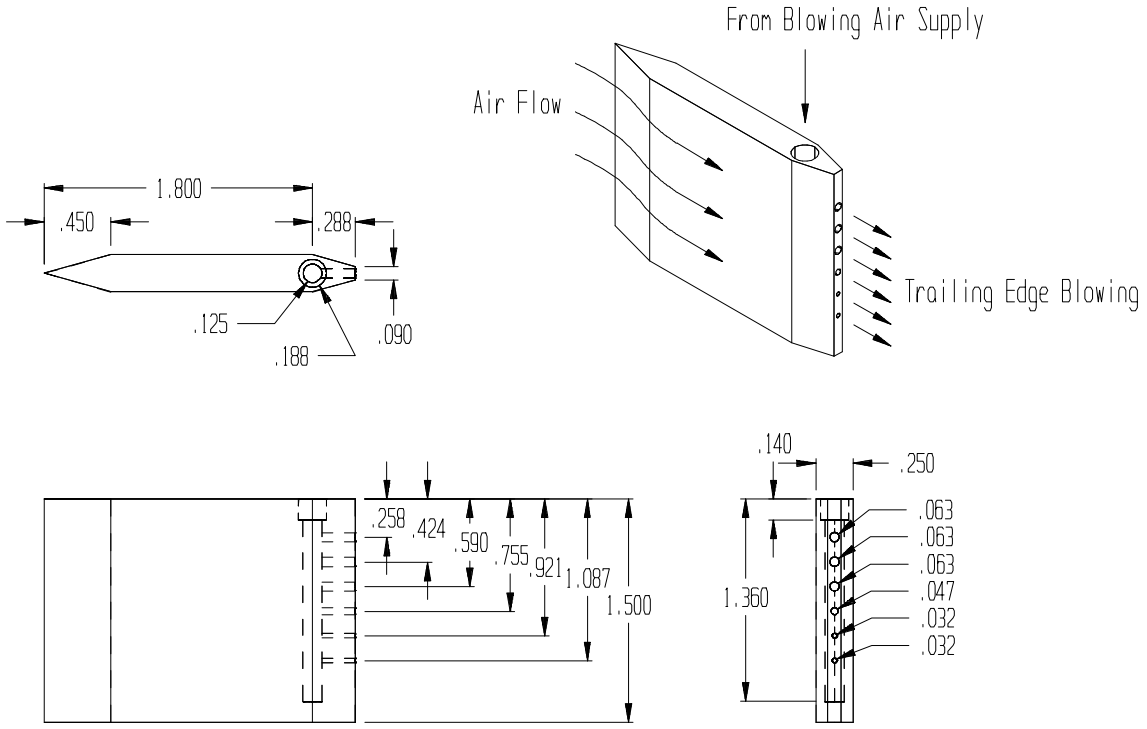

Figure 3.5 Stator Geometry (all dimensions in inches)

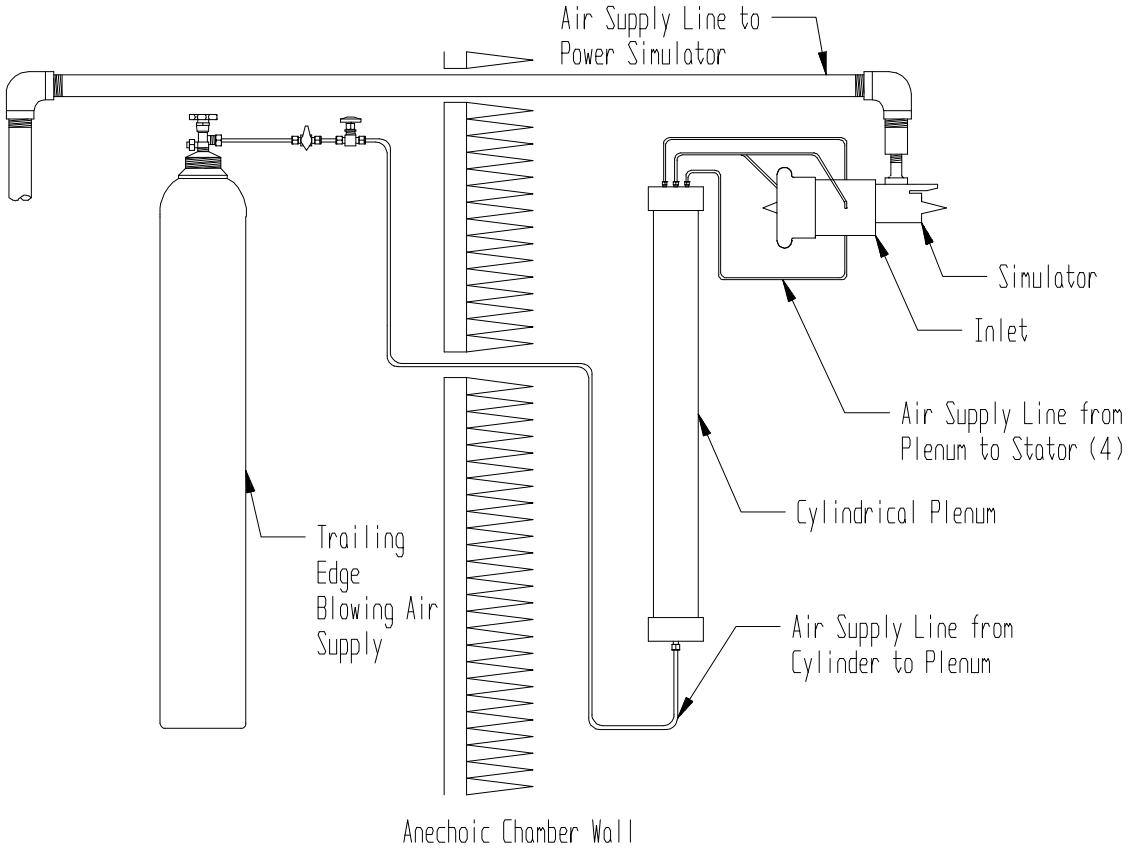

Figure 3.6 Blowing Equipment

3.3 Research Facility

All experiments involving the blowing inlet were conducted at the Virginia Tech Anechoic Chamber in the Vibrations and Acoustics Laboratory. The purpose of an anechoic chamber is to simulate free space. The chamber is designed to absorb all sound waves that impinge upon the surface of the walls. Thus, a noise source placed in an anechoic chamber will produce a sound field very similar to that which would be produced in a boundary-free space. Figure 3.7 shows the test stand in the anechoic chamber. The anechoic chamber is $13.1 \times 8.9 \times 6.6$ ft ($4.0 \times 2.7 \times 2.0$ m) with all surfaces made of Owens Corning Type 705 industrial fiberglass wedges. Each of these wedges is 3.0 ft (0.91 m) thick. An open metal grate is elevated just above the floor's wedges to provide a working surface. The Virginia Tech facility is considered anechoic above 200 Hz with an ambient noise level of approximately 30 dB. This ambient noise level is sufficiently below the noise levels of interest in this experiment. The acoustically-treated door of the anechoic chamber has an 1.5 ft (0.45 m) circular opening to provide intake air for the fan. In addition, all test stands and piping are fitted with acoustic foam to help prevent acoustic reflections from their surfaces. The Virginia Tech Anechoic Chamber is not a free-jet facility, all experiments were static tests. The stationary fan drew air into the simulator without any air flowing over the outer surface of the inlet.

The simulator-inlet rig was located in the center of the anechoic chamber, 48 in (1.2 m) from the elevated floor. As mentioned, the simulator is driven by compressed air which exhausts through a single-stage turbine having 29 blades. The high-pressure air source for the simulator is a large, four-stage reciprocating compressor. Before the air exhausts through the turbine, it passes through a heat exchanger (to cool the air) and then an activated-alumina drying unit (to remove water vapor and other contaminants from the air). The compressed air is next piped into the anechoic chamber in a 2 in (5.08 cm) pipe. The flow is manually controlled outside the anechoic chamber with a valve to adjust and maintain the rotational speed of the simulator during test runs. The exhaust from the simulator (both turbine and fan) is ducted out the rear wall of the anechoic chamber using a 12 in (30.5 cm) diameter pipe. The turbine exhaust is ducted separately from the fan exhaust so as not to effect the fan loading. Well downstream of the simulator exit, the exhausts from the turbine and fan are mixed.

3.4 Aerodynamic Measurements

The acoustic performance of an aircraft engine inlet is closely linked to its aerodynamic behavior. In order to correlate the change in acoustic performance with a corresponding change

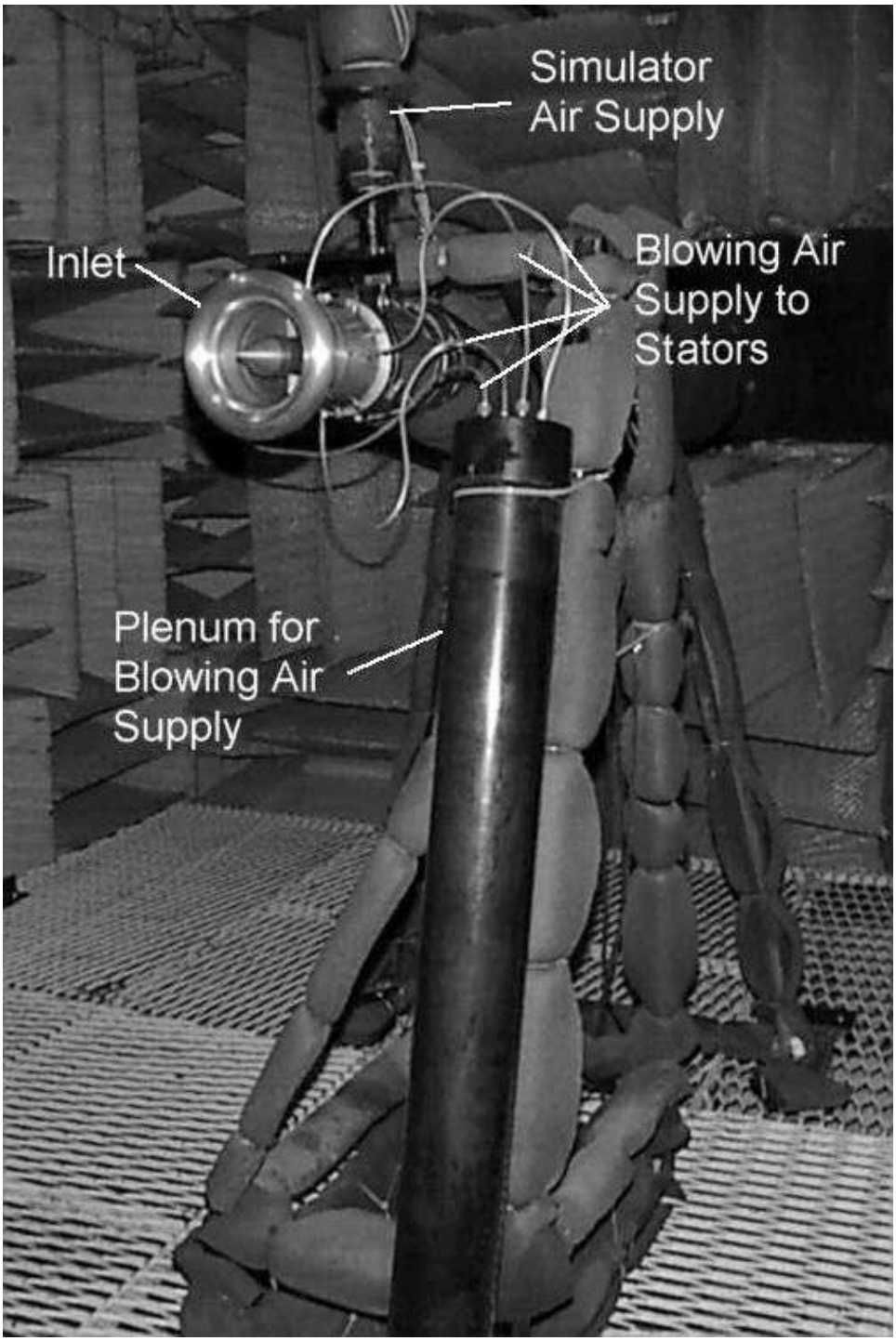

Figure 3.7 Experimental Setup in the Virginia Tech Anechoic Chamber

in flow distortion, it was essential to document the aerodynamic performance of the inlet with and without trailing edge blowing. Steady-state measurements of static and total pressure were taken to completely map the fan face and downstream wakes from the stators.

3.4.1 Aerodynamic Instrumentation

A 0.0625 inch (1.6 mm) diameter Pitot-static probe was used to measure the static and total pressures in order to calculate Mach number. In addition, a 0.125 inch (3.2 mm) diameter Kiel probe was used to make measurements of total pressure. While the Pitot-static probes measure both static and total pressure, it is critical that the probe head be aligned with the flow streamline. Unlike Pitot-static probes, Kiel probes are relatively insensitive to orientation and provide very accurate measurements of total pressure.

3.4.2 Aerodynamic Measurement Configuration

Aerodynamic measurements were made at three axial stations: behind the stators, at the fan face, and at the fan exit. The traverses behind the stators were perpendicular to the stators at three equally-spaced stations: 25% span (near the tip), 50% span (at mid span), and 75% span (near the hub). Figure 3.8 details the aerodynamic measurement locations throughout the inlet.

To examine the stator wakes, the perpendicular traverses were made at a downstream distance of 50% chord length. Because of the small scale of the inlet, it was not possible to do all three traverses (25% span, 50% span, and 75% span) on all four stators. Of the four stators, these perpendicular traverses were only done on two. All hub and tip station measurements were done on one stator and all mid span measurements were done on another. This method assumes that all of the stators produced identical trailing edge profiles. This assumption was confirmed during the bench tests and is documented in Appendix A.

Radial traverses were made in order to map out the entire fan face, which was at a downstream distance of 75% of the stator chord length from the trailing edges of the stators. The traverses at the fan face were radial traverses from the tip to hub, with each traverse comprised of seven data points. Nuckolls and Ng (1993) showed that the flows at the fan face and fan exit stations were axisymmetric. Therefore, radial traverses were made at only five circumferential

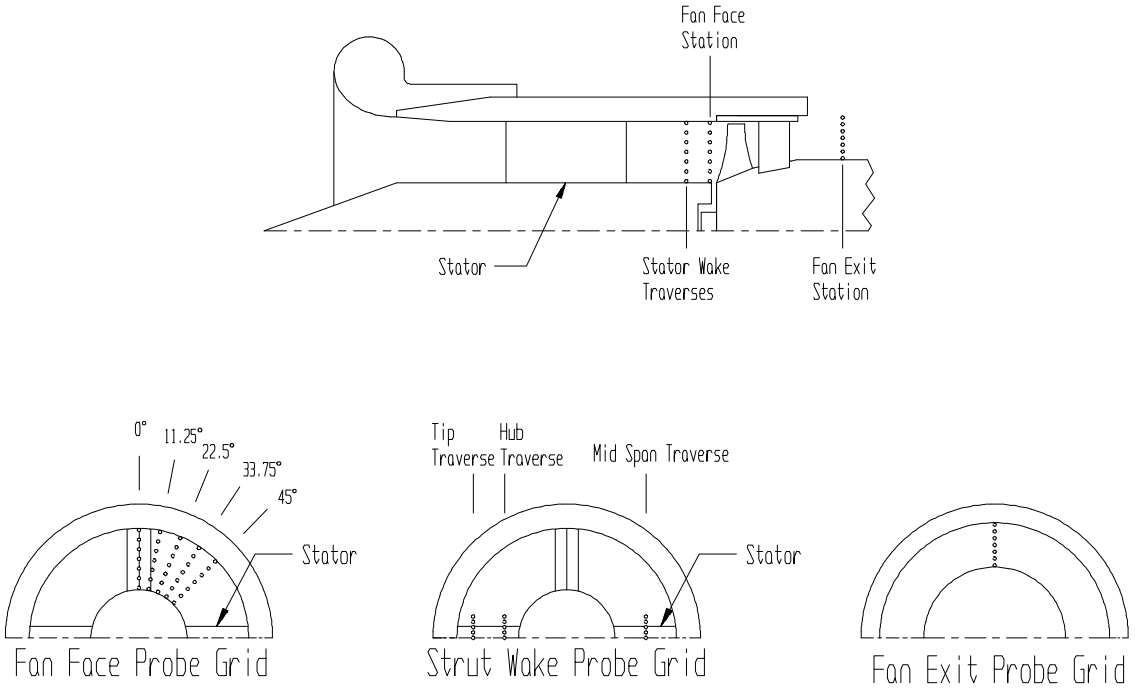

Figure 3.8 Aerodynamic Measurement Locations

locations. These five circumferential locations were at equally spaced angles between 0° and 45°.

3.5 Acoustic Measurements

The key measurements in this study were the acoustic measurements. Any change in the rotor-stator interaction directly impacts the acoustic characteristics of the inlet. In order to record these changes, acoustic measurements were taken at one radius in the far field over an angle of 0° to 110°.

3.5.1 Acoustic Instrumentation

A Bruel and Kjaer Model 4136 condenser microphone was used for all acoustic measurements. The microphone has a 0.25 in (6.4 mm) diameter diaphragm which provided linear response up to 30,000 Hz. The microphone was connected to a preamp and then a battery powered Bruel and Kjaer power supply. A Bruel and Kjaer Model 2030 spectrum analyzer was then used to process the signal from the microphone. Prior to testing, the microphone was calibrated using a Bruel and Kjaer pistophone which produced a 94 dB sound pressure level at 1000 Hz.

The signal analyzer produced a narrowband frequency spectrum from 0 to 25,600 Hz with a bandwidth of 32 Hz. From each of these spectrums, the sound pressure level of the blade passing frequency (BPF) and the overall sound pressure level (OASPL) were obtained. The overall sound pressure level is the summation of the sound pressure levels for the frequencies from 0 to 25,600 Hz. To account for the variation inherent to these acoustic measurements, 20 spectrums were linearly averaged to produce one measurement for a given position, configuration, and speed. Next, five of these measurements were taken and averaged to yield the sound pressure level for a particular position. In total, the sound pressure level was measured 100 times and averaged to yield each data point.

3.5.2 Acoustic Measurement Configuration

Acoustic measurements were taken at 12 points along a circular arc ranging from 0° to 110° at a horizontal distance of 48 in (1.22 m) from the cowl lip of the inlet. The microphone was elevated 48 in (1.22 m) from the floor for all measurements with the diaphragm pointing directly at the inlet. Figure 3.9 illustrates the acoustic measurement locations.

3.6 Test Matrix

These experiments were conducted at three different simulator speeds which correspond to three different flight conditions: 30,000 RPM (40 PNC), 50,000 RPM (60 PNC), and 70,000 RPM (88 PNC). For the 30,000 RPM (40 PNC) and 50,000 RPM (60 PNC) cases both aerodynamic and acoustic data were taken. At 70,000 RPM (88PNC) only acoustic data was taken. A shaft speed of 50,000 RPM (60 PNC) corresponds to landing approach conditions, while 70,000 RPM (88 PNC) corresponds to takeoff conditions when the engine experiences its maximum loading. Each of these speeds was tested with and without blowing.

In order to gain some understanding of the entire radiated field, acoustic measurements were taken for two different measurement planes in the inlet. This secondary measurement plane was tested with and without blowing at only two speeds, 30,000 RPM (40 PNC) and 50,000 RPM (60 PNC). Figure 3.10 shows the primary and secondary measurement planes.

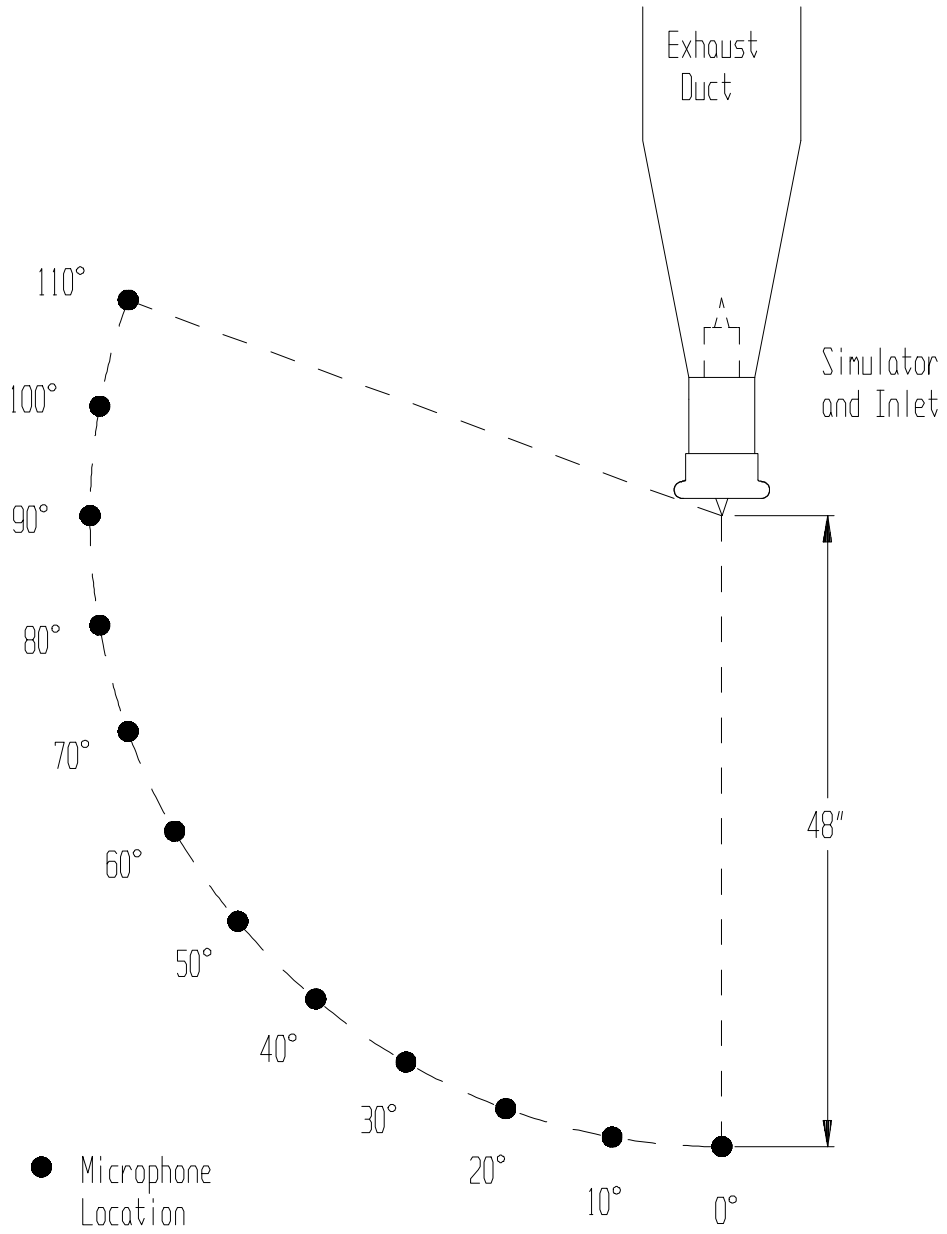

Figure 3.9 Acoustic Measurement Locations

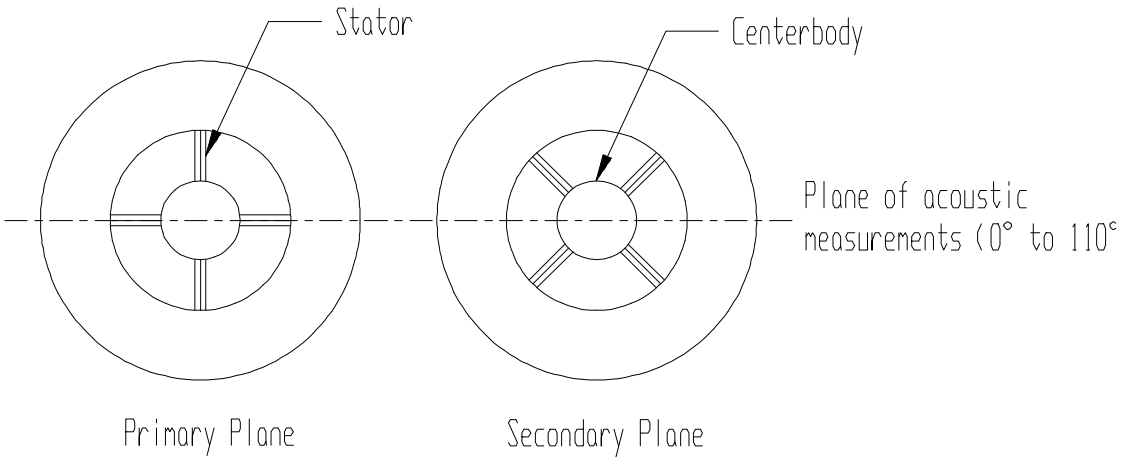

Figure 3.10 Primary and Secondary Planes

4.0 Results and Discussion

This chapter is divided into two sections, the first detailing the aerodynamic results and the second detailing the acoustic results. These results include data taken at speeds of 30,000 RPM (40 PNC), 50,000 (60 PNC), and 70,000 RPM (88 PNC) all with and without blowing from the trailing edges of the four upstream stators. The acoustic tests at 30,000 RPM (40 PNC) and 50,000 RPM (60 PNC) were performed on both the primary and secondary planes. For the turbofan simulator used in this experiment a speed of 50,000 RPM (60 PNC) corresponds to approach conditions, while 70,000 RPM (88 PNC) simulates takeoff conditions.

The blowing rate for each speed was chosen based upon acoustic results from two microphone positions. One microphone was placed at the 20° position in the far field and another was placed at the 80° position. At each test speed the overall and tone sound pressure levels were measured without blowing and then with different blowing rates. The noise reduction at each position for each blowing rate was examined, and an optimum blowing rate was chosen. Appendix B details this process.

4.1 Aerodynamic Results

As mentioned in Chapter 3.4.2, aerodynamic measurements were taken at two axial locations: at the fan face (a downstream distance of 75% stator chord length) and perpendicular to the stators (a downstream distance of 50% of the stator chord length). At the fan face radial traverses were made at five equally-spaced circumferential locations ranging from 0° to 45° around the inlet. Assuming the flow field to be symmetric, these measurements were mirrored to describe the flow over the entire fan face. The traverses perpendicular to the stators were made at three equally-spaced radial locations: 25% span (near the tip), 50% span (mid span), and 75% span (near the hub). All three of these locations were not measured on all four stators. After

showing that all four stators performed similarly, the 25% span and 75% span stations were measured on one stator and the 50% span station was measured on another.

4.1.1 Inlet Flow Distortion

Flow distortion at the fan face is a significant contributor to fan noise, and the primary cause of fan face distortion is the stators. The focus of this research is to use wake management to re-energize the stators' wakes and reduce the flow distortion at the fan face. In this section, contour plots of the Mach number at the fan face are used to illustrate how blowing from the trailing edges of the stators effects the flow distortion at the fan face.

It is important to note that there is more than one type of distortion that affects the acoustic performance of an engine. Figure 4.1 illustrates two hypothetical examples of flow distortion. The top figure illustrates flow distortion with gradients only in the radial direction. At a given radius on the blade, that part of the blade experiences a constant velocity and constant pressure throughout one complete rotation. The subsequent force on each radial section of the blade does not change. Since the blade remains uniformly loaded, noise generation is minimal. The second contour plot in Figure 4.1 exhibits gradients only in the circumferential direction. As a blade rotates through this type of distortion its loading depends upon the angular position of the blade. For a blade rotating at a constant angular velocity this loading will be periodic, and the fan will radiate noise at multiples of the blade passing frequency. It is this circumferential distortion, not radial, that is responsible for the blade passing tone.

Figures 4.2 and 4.3 compare the Mach number contours with and without blowing at 30,000 RPM (40 PNC) and 50,000 RPM (60 PNC), respectively. At both 40 PNC and 60 PNC a portion of each stator wake is removed with the use of trailing edge blowing. Similar to the gradients on the lower contour plot in Figure 4.1, the stator wakes result in circumferential distortion. As fan blades rotate through the stator wakes, the blades experience unsteady loading. By re-energizing parts of the stator wakes, the sources of unsteady loading on the blades have been reduced. On all of the contour plots, note the region near the hub where the Mach number is much lower compared to the rest of the flow. This was observed at both 40 PNC and 60 PNC with and without blowing. It is believed that there is a region of flow separation near the hub resulting from the nose cone. As the flow moves over the nose cone and is turned toward the axial direction, it separates and is not able to reattach before encountering the stators.

It is often convenient to quantify distortion through the use of a distortion parameter. A distortion parameter was developed to quantify the gradient of the total pressure losses in the circumferential direction. This parameter is defined in the Aerospace Recommended Practice

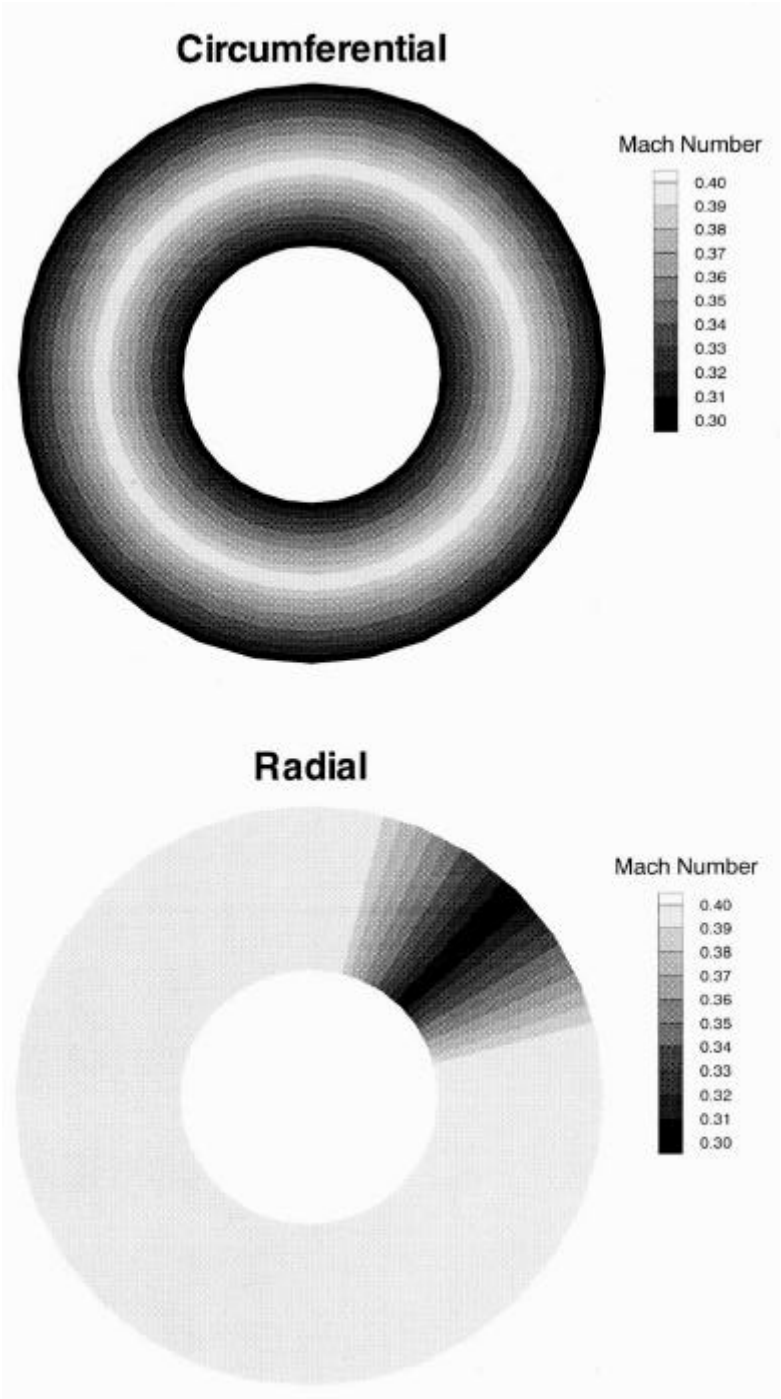

Figure 4.1 Hypothetical Gradients of Mach Number Distortion at the Fan Face

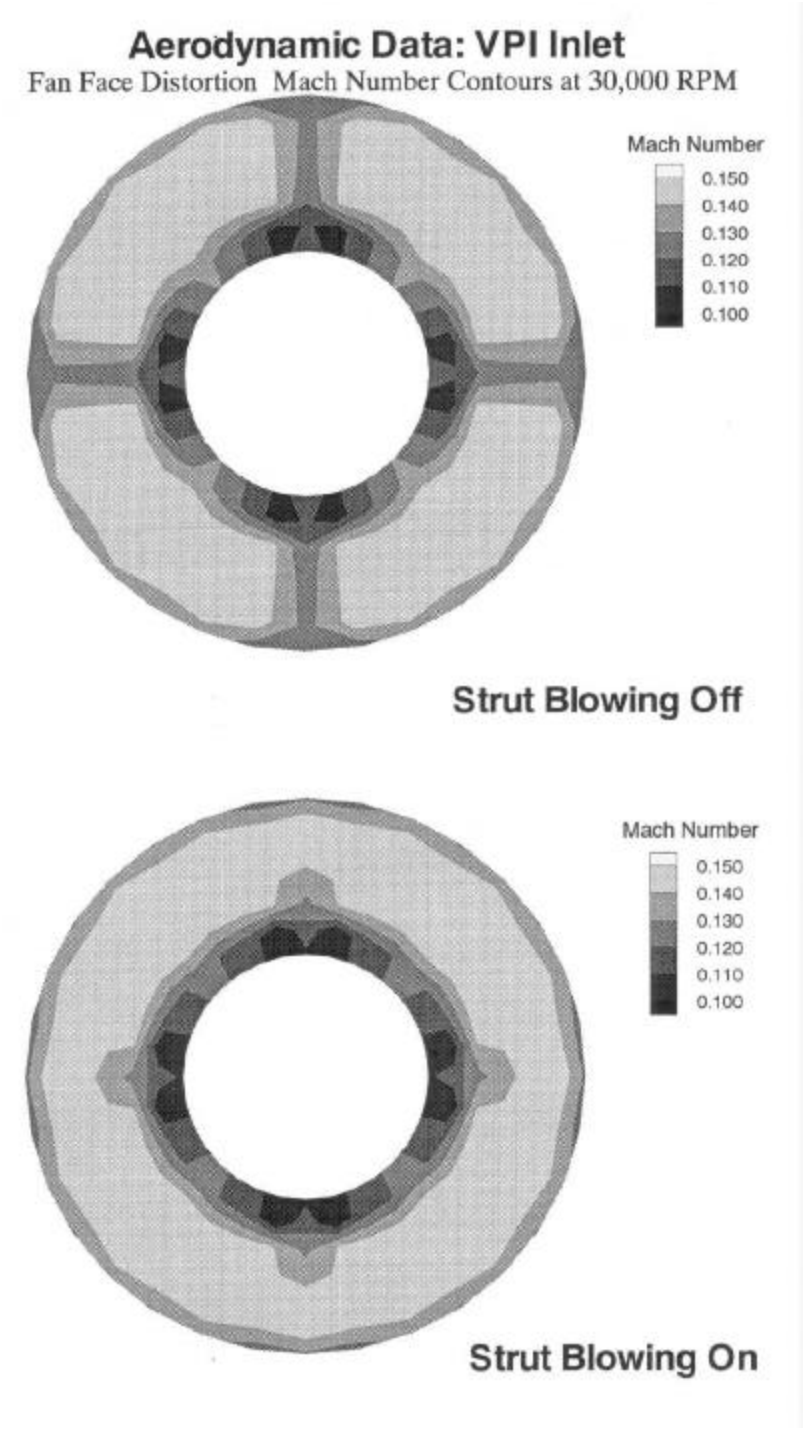

Figure 4.2 Mach Number Distribution at the Fan Face, 40 PNC

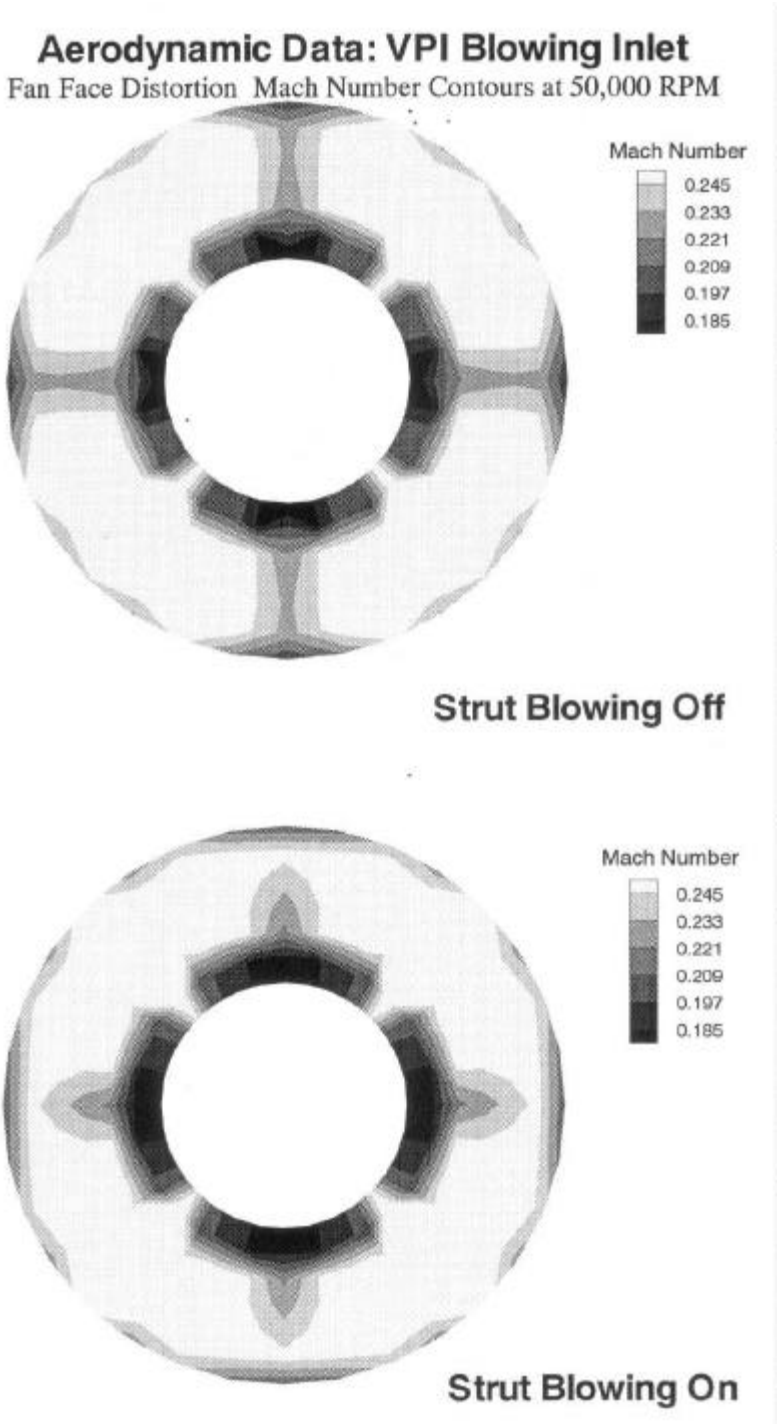

Figure 4.3 Mach Number Distribution at the Fan Face, 60 PNC

(ARP 1420) by the Society of Automotive Engineers. The distortion parameter describes the magnitude of the total pressure defect for each radial ring of measurements spanning the entire 360° annulus. The distortion parameter was calculated for each radial position and then area-averaged to give the overall circumferential distortion for the fan face. Table 4.1 gives the distortion at each of the simulator test speeds (40 PNC and 60 PNC). Note that using trailing edge blowing reduced the circumferential distortion more at 50,000 RPM (60 PNC) than 30,000 RPM (40 PNC).

Table 4.1 Circumferential Distortion Parameter at the Fan Face

Simulator Test Speed	Distortion Parameter Without Blowing	Distortion Parameter With Blowing	Percent Reduction
30,000 RPM (40 PNC)	0.103%	0.0799%	22.4%
50,000 RPM (60 PNC)	0.252%	0.171%	32.1%

4.1.2 Inlet Pressure Recovery

The aerodynamic performance of an aircraft engine inlet is often stated in terms of total pressure recovery. Defined as $\frac{P_t}{P_{t,ambient}}$, total pressure recovery is a measure of the losses that the fluid incurs during its flow through the inlet. A total pressure recovery of 1.0 would indicate isentropic flow. Figures 4.4 and 4.5 show total pressure contours at 30,000 RPM (40 PNC) and 50,000 RPM (60 PNC), respectively. Note the region of low total pressure recovery near the hub. As in the Mach number contours, there appears to be substantial flow separation in this region. Because of this separation, trailing edge blowing appears to have little effect on the total pressure at the hub. However, there is a significant reduction in the stator wakes from the mid span of the stators outward.

4.1.3 Stator Wake Management

The traverses perpendicular to the stators provide the most insight as to how the trailing edge blowing effects the stators' wakes. Figures 4.6 and 4.7 show the total pressure profiles

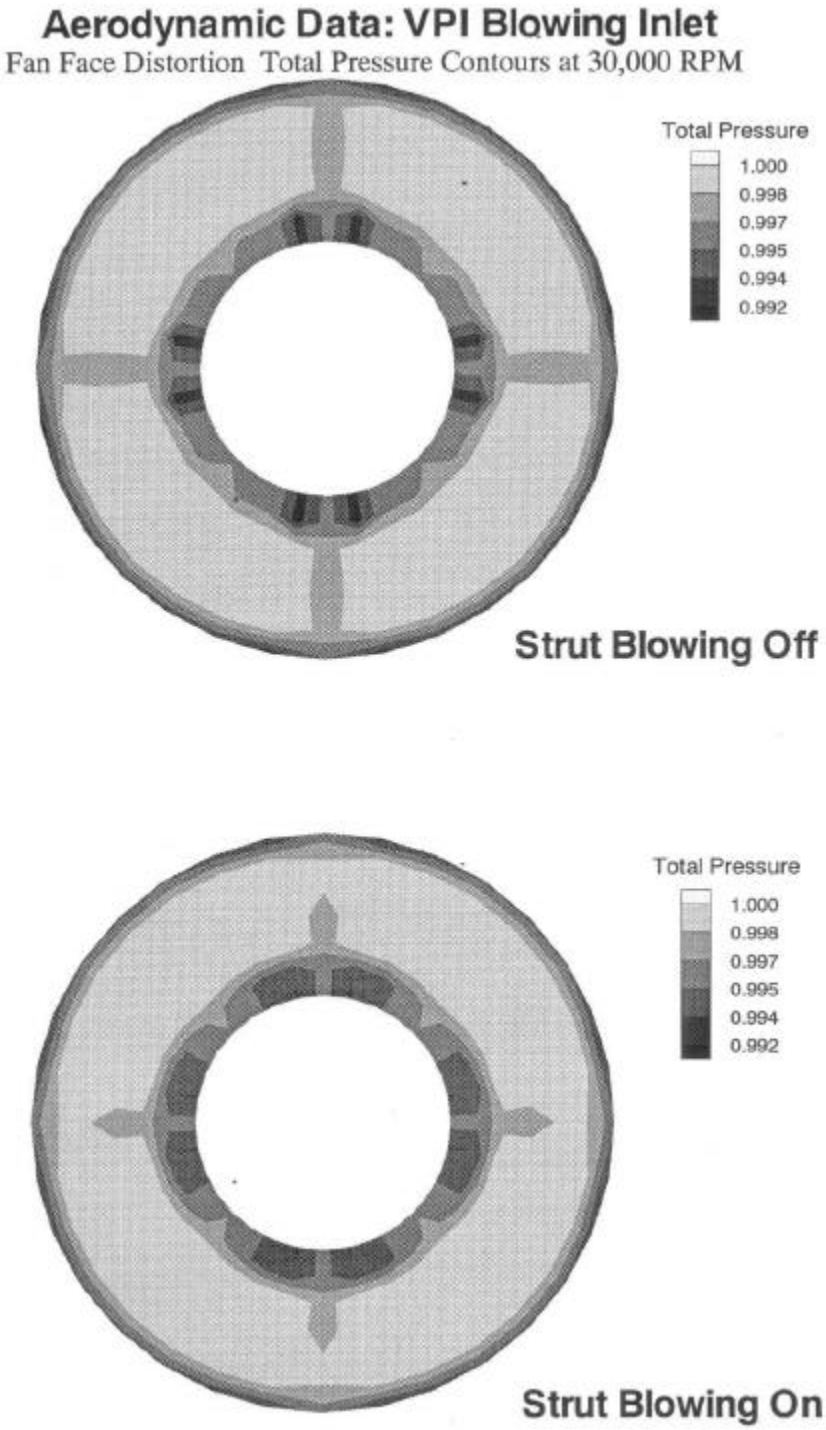

Figure 4.4 Total Pressure Distribution at the Fan Face, 40 PNC

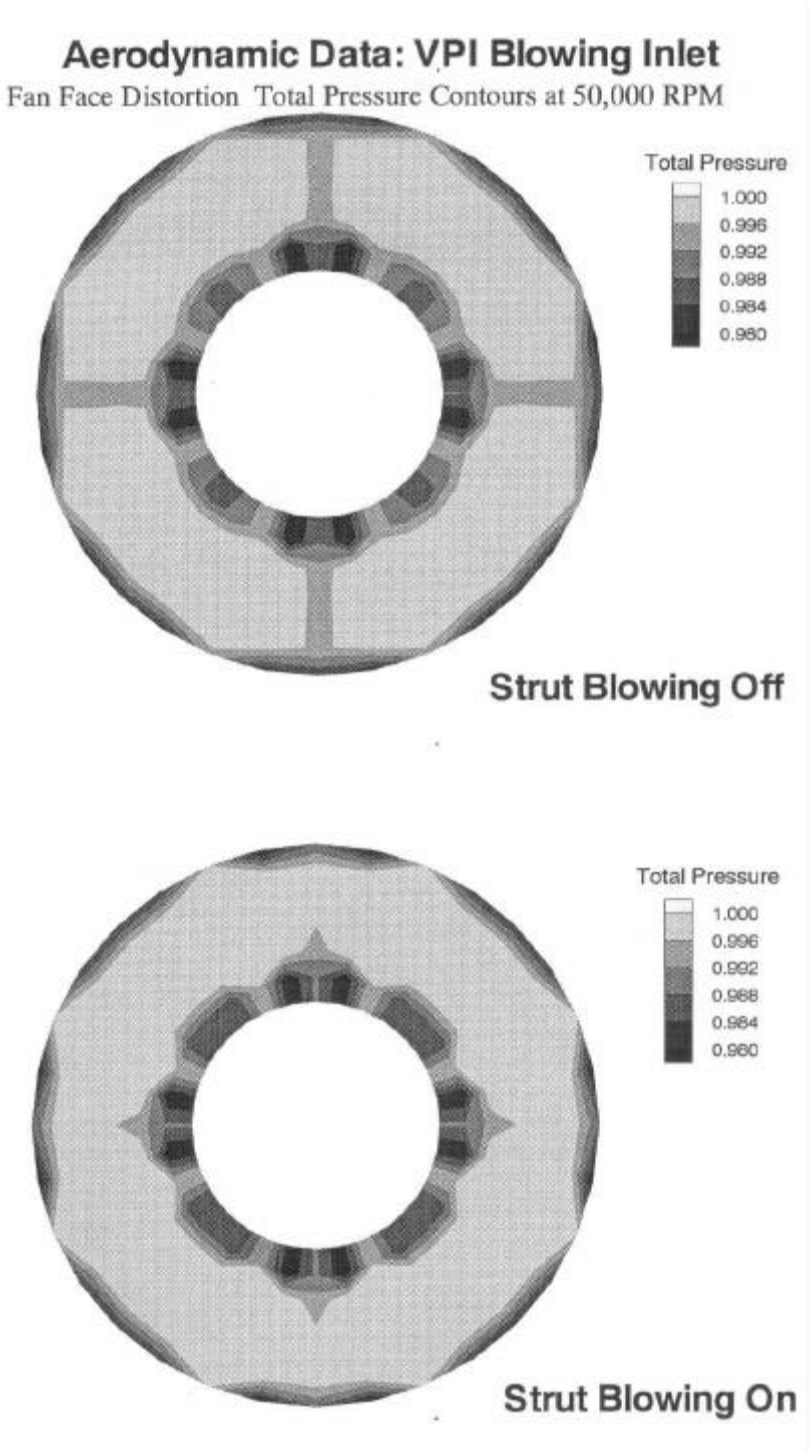

Figure 4.5 Total Pressure Distribution at the Fan Face, 60 PNC

behind the stators at 30,000 RPM (40 PNC) and 50,000 (60 PNC), respectively. These traverses were done at three positions: 25% span (near the tip), 50% span (at the mid span), and 75% (and the hub). Note that the wakes at 60 PNC are roughly twice as deep as those at 40 PNC. Compared to 60 PNC, trailing edge blowing is slightly more effective at 40 PNC. As the speed increases the wakes develop much deeper, and it becomes more difficult to completely re-energize the wakes. With the severe total pressure deficit at the hub, trailing edge blowing has little effect on the stators' wakes.

4.1.4 Fan Operation Conditions

Noise from a fan is a function of fan loading. In order to draw any conclusions about whether trailing edge blowing from the stators reduces the radiated noise, it is necessary to determine the effect of the blowing on the fan operating point. Total pressure measurements were made at the fan exit in order to determine the total pressure ratio for the fan. The pressure measurements at the fan face and fan exit were both area-averaged in calculating the pressure ratio. Table 4.2 shows that using trailing edge blowing did not alter the fan pressure ratio at either 30,000 RPM (40 PNC) or 50,000 RPM (60 PNC).

Table 4.2 Total Pressure Ratio

Simulator Test Speed	Without Blowing	With Blowing
30,000 RPM (40 PNC)	1.07	1.07
50,000 RPM (60 PNC)	1.19	1.19

With the same total pressure ratios (1.07 at 40 PNC and 1.19 at 60 PNC), the operating conditions and loading for the fan were the same. Had the operating point changed with the addition of trailing edge blowing from the stators, it would not have been appropriate to compare the acoustic results with blowing and without blowing. With the same operating point, the blowing and no blowing cases can be considered to have the same noise source.

The mass flow added due to blowing is an important consideration. If an enormous amount of blowing is required, it will likely add complexity to the system. For blowing to be feasible in a real engine, the amount of air required to re-energize the wakes must be relatively small. For the same simulator speed and exit area in these experiments, the fan pressure ratio did not change noticeably. This is an indicator that the amount of mass flow added was negligible in comparison to the overall fan mass flow. Obviously, the upper bound on the mass flow from the

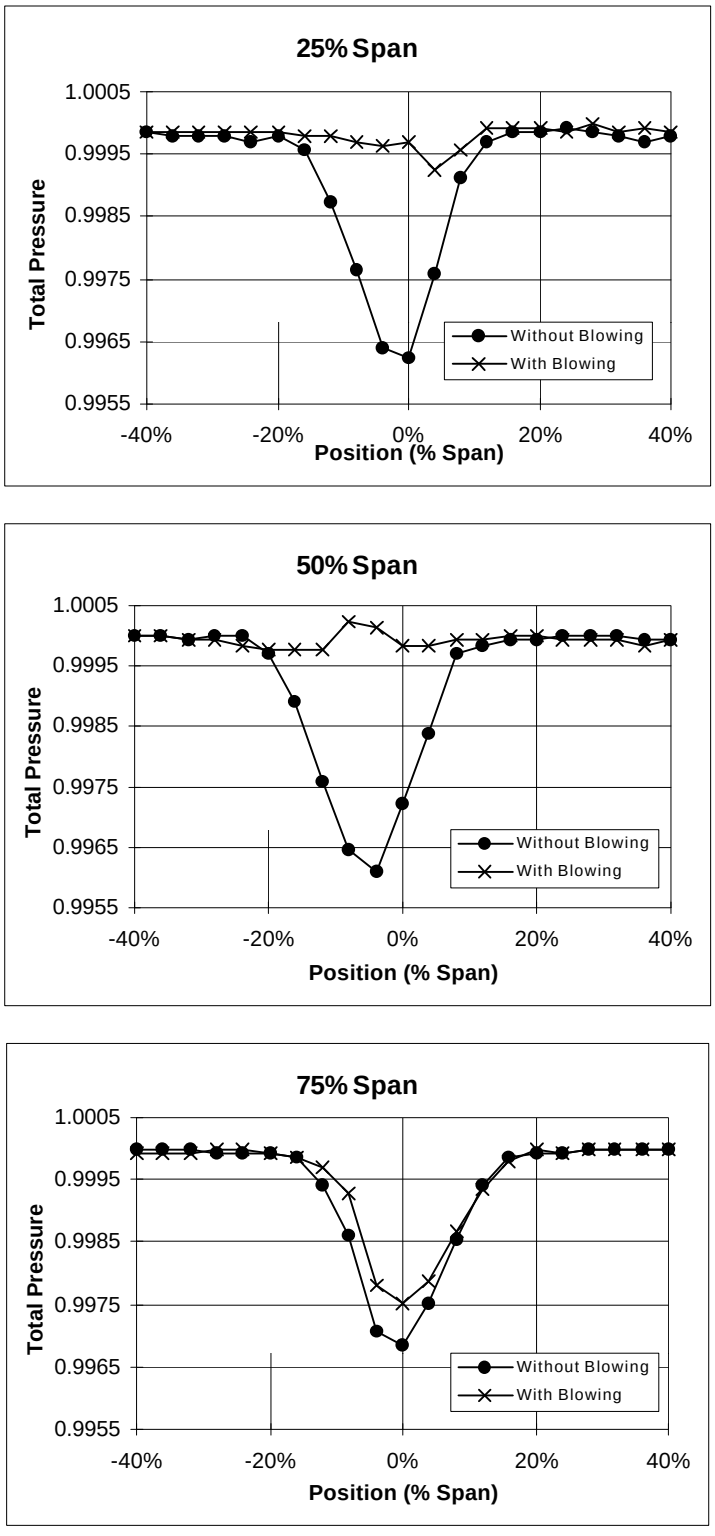

Figure 4.6 Wake Behind the Stator, 40 PNC

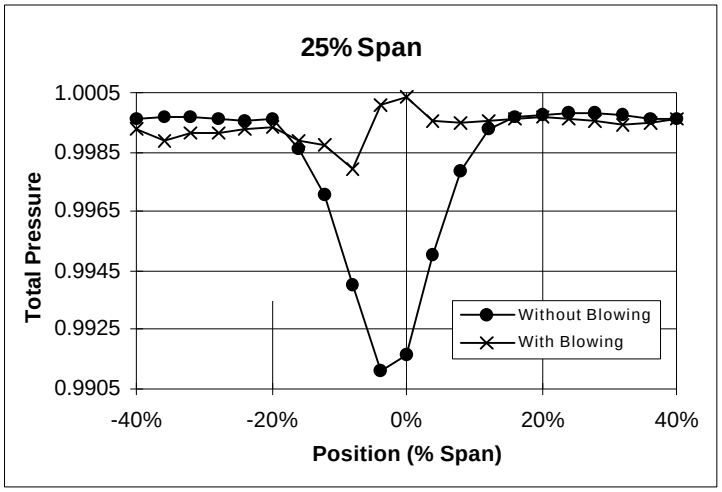

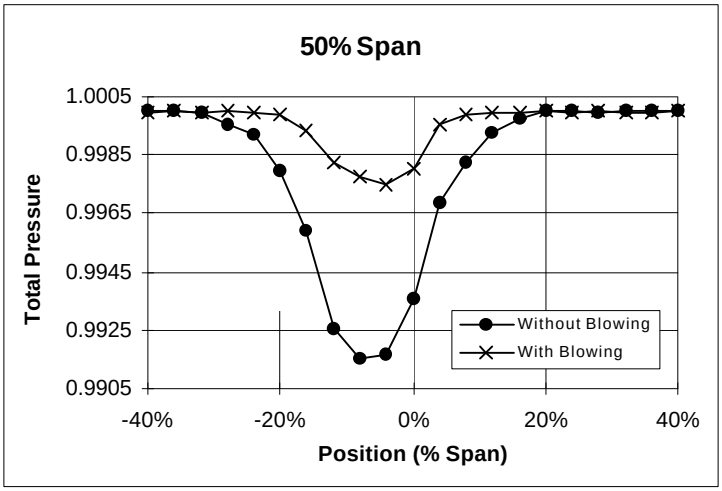

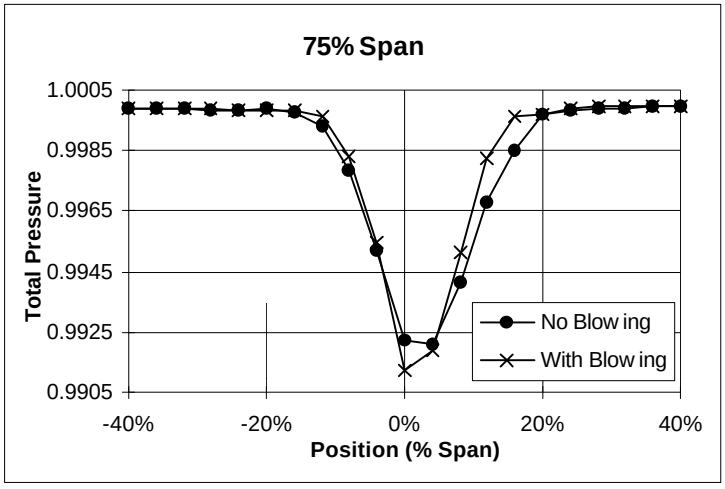

Figure 4.7 Wake Behind the Stator, 60 PNC

stators is when the trailing edge holes are choked. Even for this scenario, the amount of mass flow added would approximately 1.5% of the overall fan mass flow. Figures 4.6 and 4.7 indicate that the trailing edge holes are not close to being choked, so the amount of mass flow added due to blowing is negligible.

4.2 Acoustic Results

Far field acoustic data was taken at twelve angular positions from 0° to 110° at a distance of four feet from the inlet. These results are presented in three sections. First, sample acoustic spectra are examined. In the second section the radiated patterns are presented. In the last section the modal analysis described in Chapter 2 is applied to this inlet's geometry and operating conditions.

4.2.1 Narrowband Spectra

In order to get a detailed description of the noise source in this experiment, narrowband acoustic spectra were recorded with and without blowing at each of the 12 angular positions. The spectra recorded the sound pressure level from 0 to 25,600 Hz with a bandwidth of 32 Hz.

Figures 4.8, 4.9, and 4.10 illustrate acoustic spectra at 30,000 RPM (40 PNC), 50,000 RPM (60 PNC), and 70,000 RPM (88 PNC), respectively. As is common among fans with subsonic blade tip velocities, the blade passing tone dominates the spectra at 30,000 RPM (40 PNC) and 50,000 RPM (60 PNC). With the exception of the blade passing frequency and its harmonics, the acoustic energy is relatively equally distributed among all of the frequencies in the spectrum. This broadband noise can be caused by boundary layer turbulence, interaction of the blade pressure fields with inlet turbulence, and interaction between the blade pressure fields and wall boundary layer.

At 30,000 RPM (40 PNC), the blade passing tone occurs at 9,000 Hz, and the blade tip Mach number is 0.48. The first harmonic of the blade passing frequency is also prominent at 18,000 Hz.

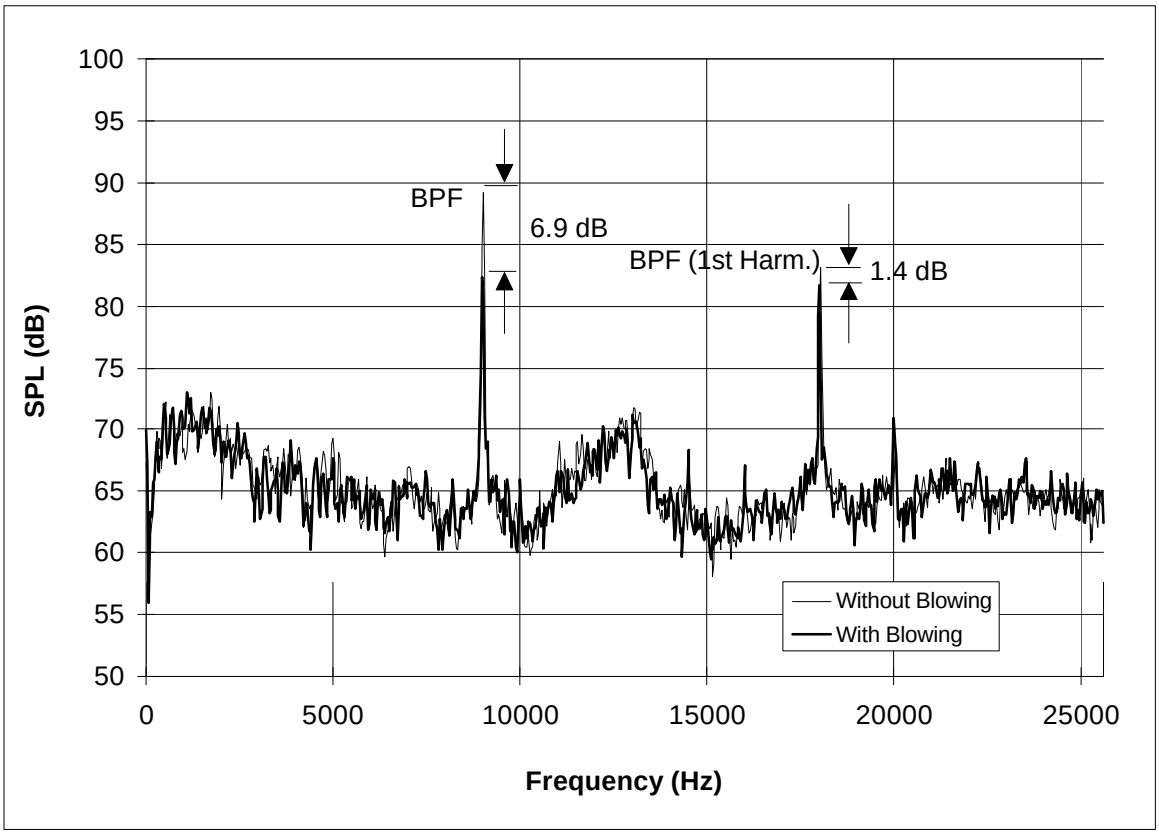

Figure 4.8 Sample Acoustic Spectrum at 40 PNC, 90° Microphone Location

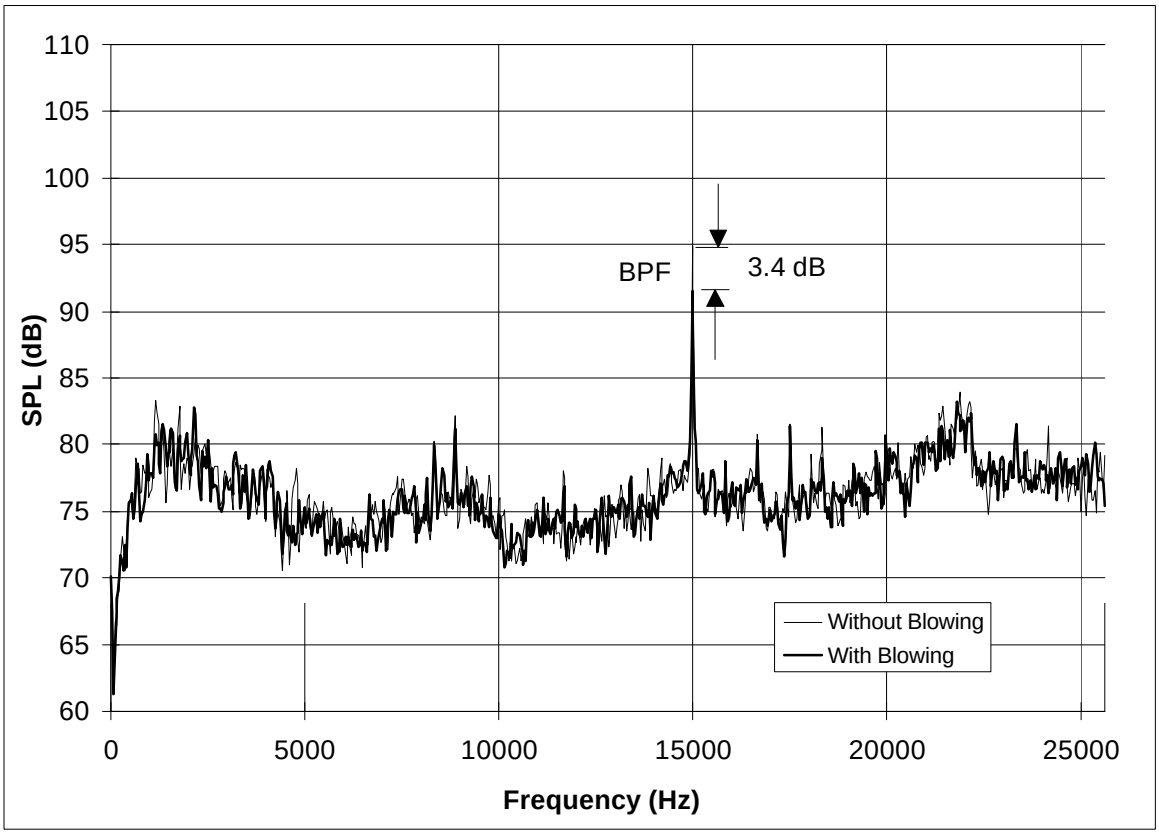

Figure 4.9 Sample Acoustic Spectrum at 60 PNC, 90° Microphone Location

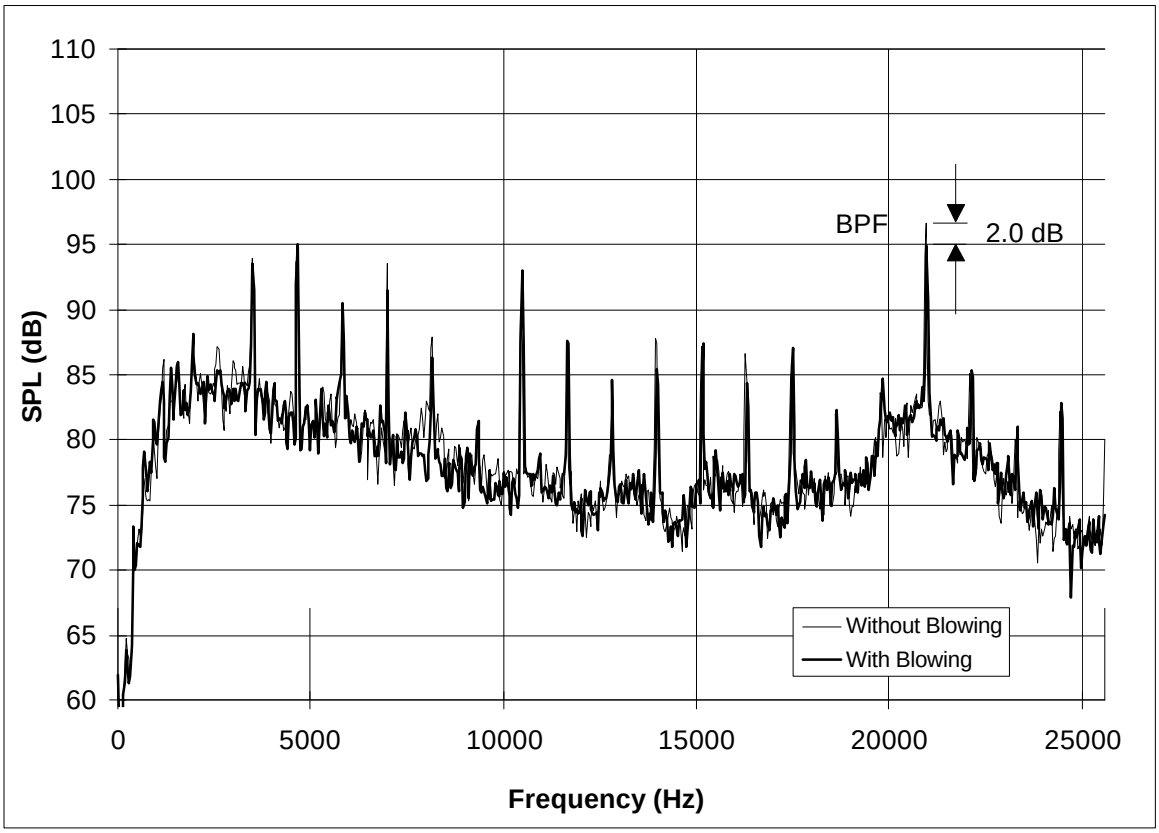

Figure 4.10 Sample Acoustic Spectrum at 88 PNC, 90° Microphone Location

The acoustic spectrum at 50,000 RPM (60 PNC) shows the blade passing tone at 15,000 Hz. Because the upper limit of the spectrum was 25,600 Hz, no harmonics of the BPF are recorded. At 50,000 (60 PNC) the blade tip Mach number is 0.8.

For the acoustic spectra at 70,000 RPM (88 PNC), note the series of peaks that occur at 1167 Hz intervals. This noise is known as combination tone noise, multiple pure tone noise, or "buzz-saw" noise, and is the result of supersonic relative tip Mach numbers of the rotating fan blades. At 70,000 RPM (88 PNC) the blade tip Mach number is 1.12. For each of the rotating blades, a shock wave is established in front of the blade. However, due to the nonlinear nature of shocks and the normal manufacturing tolerances between each of the blades, there are small deviations between the shock wave amplitudes and spacing. The result is that the noise spectra have harmonics of the fan rotational frequency. For this simulator (18 blades at 70,000 RPM), the harmonics occur at 1167 Hz intervals. The energy for the combination tones is transferred from the blade passing frequency and its harmonics to the frequencies which are integer multiples of the fan rotation frequency.

As expected, trailing edge blowing reduced the tone SPL at each of the speeds. In addition, the use of trailing edge blowing had little effect on the broadband noise. Since the purpose of trailing edge blowing is to reduce only the circumferential distortion, it is understandable that most of the improvement is observed in the tone SPL and not the broadband noise. Note that as the speed increases, the tone is reduced less. The wakes become deeper with increasing flow velocity, and it becomes much more difficult to re-energize the wakes. At 70,000 RPM (88 PNC) trailing edge blowing is able to reduce some of the multiple pure tones. It is suspected that the extreme nonlinearity of the shocks coupled with the manufacturing tolerances of the blades cause some of the combination tones to be reduced and some to be increased by trailing edge blowing.

4.2.2 Radiated Noise Patterns

The key results of the experiment are presented in this section. In order to characterize the radiation pattern of the complex noise source used in this experiment, acoustic measurements were taken at 12 different locations from 0° to 110° at a distance of 48 in. In this experiment, 0° was along the axis of the inlet.

Figure 4.11 shows how trailing edge blowing from the stators effects the radiated tone and overall sound pressure levels for the primary plane at 30,000 RPM (40 PNC). These values are shown in Tables 4.3 and 4.4. The top graph represents the sound pressure level at the blade passing frequency only, in this case 9,000 Hz. Note the significant reduction of the tone SPL at

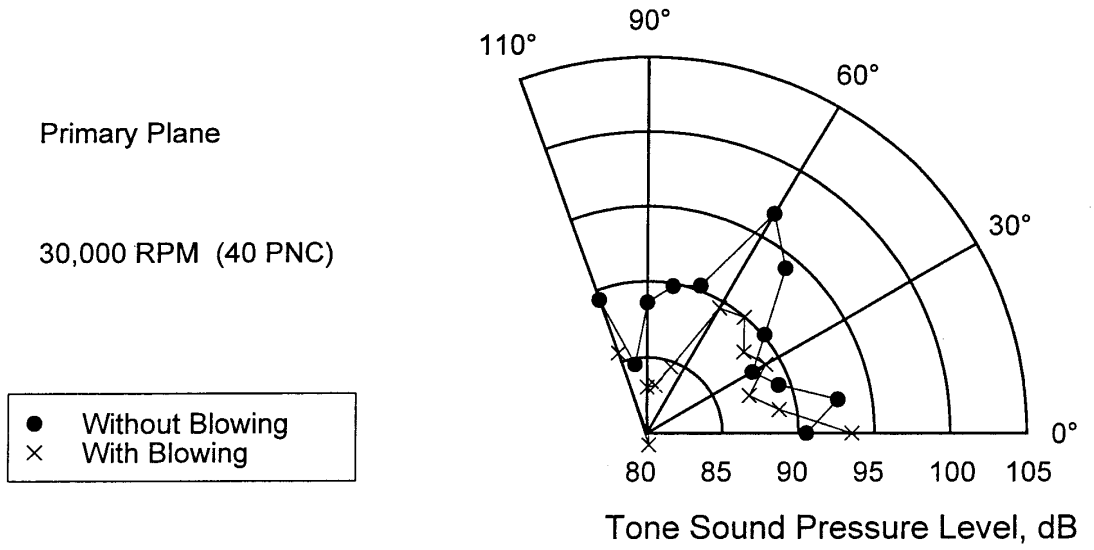

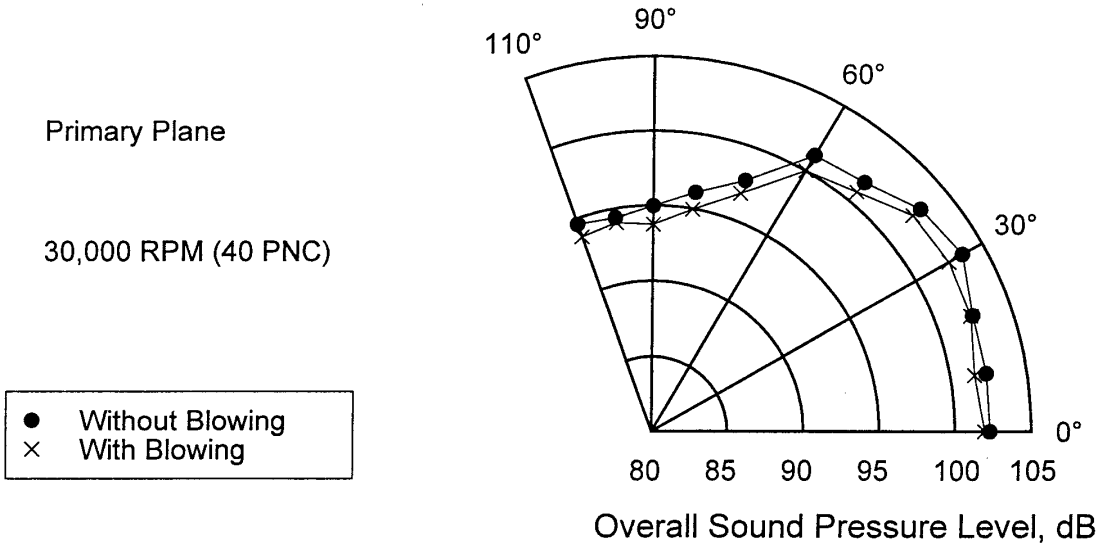

Figure 4.11 Directivity Plots at 40 PNC, Primary Plane

some locations. At 50° the tone SPL was reduced by 7.2 dB, and from 50° to 110° the tone was reduced by an average of 5.6 dB. The average sound pressure level was calculated from

$$SPL_{avg} = 10\log_{10}\left[\frac{1}{n}\sum_{i=1}^{n} 10^{\left(\frac{SPL_i}{10}\right)}\right] \tag{4.1}$$

The overall sound pressure level, shown in Figure 4.11 represents the summation over the entire frequency range. The overall SPL was reduced by approximately 1 dB at each position. At no point did the trailing edge blowing increase the overall SPL. Tables 4.3 and 4.4 show the data for the plots.

Table 4.3 Tone SPL for the Primary Plane at 30,000 RPM (40 PNC)

Microphone Position	Tone SPL (dB) Without Blowing	Tone SPL (dB) With Blowing	SPL Reduction (dB) Without - With Blowing
0°	90.5	93.5	-3.0
10°	92.8	88.9	3.9
20°	89.3	87.2	2.1
30°	88.0	89.1	-1.0
40°	90.1	88.3	1.8
50°	94.2	90.0	4.2
60°	96.7	89.5	7.2
70°	90.3	84.6	5.7
80°	89.8	83.2	6.7
90°	88.6	83.0	5.6
100°	84.6	79.2	5.4
110°	89.4	85.6	3.7

Table 4.4 Overall SPL for the Primary Plane at 30,000 RPM (40 PNC)

Microphone Position	Tone SPL (dB) Without Blowing	Tone SPL (dB) With Blowing	SPL Reduction (dB) Without - With Blowing
0°	102.3	102.0	0.4
10°	102.4	101.6	0.8
20°	102.5	102.3	0.1
30°	103.5	102.5	1.0
40°	102.9	102.3	0.6
50°	101.6	100.8	0.8
60°	101.2	100.0	1.2
70°	97.8	96.8	0.9
80°	96.1	95.0	1.2
90°	95.0	93.7	1.2
100°	94.4	94.1	0.3
110°	94.6	93.7	0.9

Figure 4.12 shows the directivity plots for the secondary plane at 30,000 RPM (40 PNC). Tables 4.5 and 4.6 show the data for these plots. At 80° the tone SPL was reduced by 8.9 dB, and was reduced by an average of 6.15 dB between 30° and 90°. As with the primary plane, the overall SPL in the secondary plane was reduced by approximately 1 dB at each position. Again, trailing edge blowing did not increase the overall SPL at any locations.

Table 4.5 Tone SPL for the Secondary Plane at 30,000 RPM (40 PNC)

Microphone Position	Tone SPL (dB) Without Blowing	Tone SPL (dB) With Blowing	SPL Reduction (dB) Without - With Blowing
0°	88.2	92.2	-4.1
10°	88.5	90.3	-1.8
20°	94.8	91.4	3.4
30°	95.7	89.2	6.5
40°	94.4	89.6	4.8
50°	97.2	90.7	6.6
60°	97.2	90.6	6.6
70°	96.8	92.8	4.0
80°	93.5	84.6	8.9
90°	92.2	89.0	3.3
100°	81.6	84.2	-2.7
110°	88.6	83.7	5.0

Table 4.6 Overall SPL for the Secondary Plane at 30,000 RPM (40 PNC)

Microphone Position	Overall SPL (dB) Without Blowing	Overall SPL (dB) With Blowing	SPL Reduction (dB) Without - With Blowing
0°	102.9	102.5	0.5
10°	103.5	103.2	0.2
20°	103.8	103.1	0.7
30°	103.8	102.8	1.0
40°	102.8	101.8	1.0
50°	102.9	101.1	1.8
60°	103.1	101.2	1.9
70°	101.8	100.3	1.6
80°	98.8	96.5	2.3
90°	96.5	94.6	1.9
100°	93.9	93.7	0.2
110°	94.7	93.5	1.2

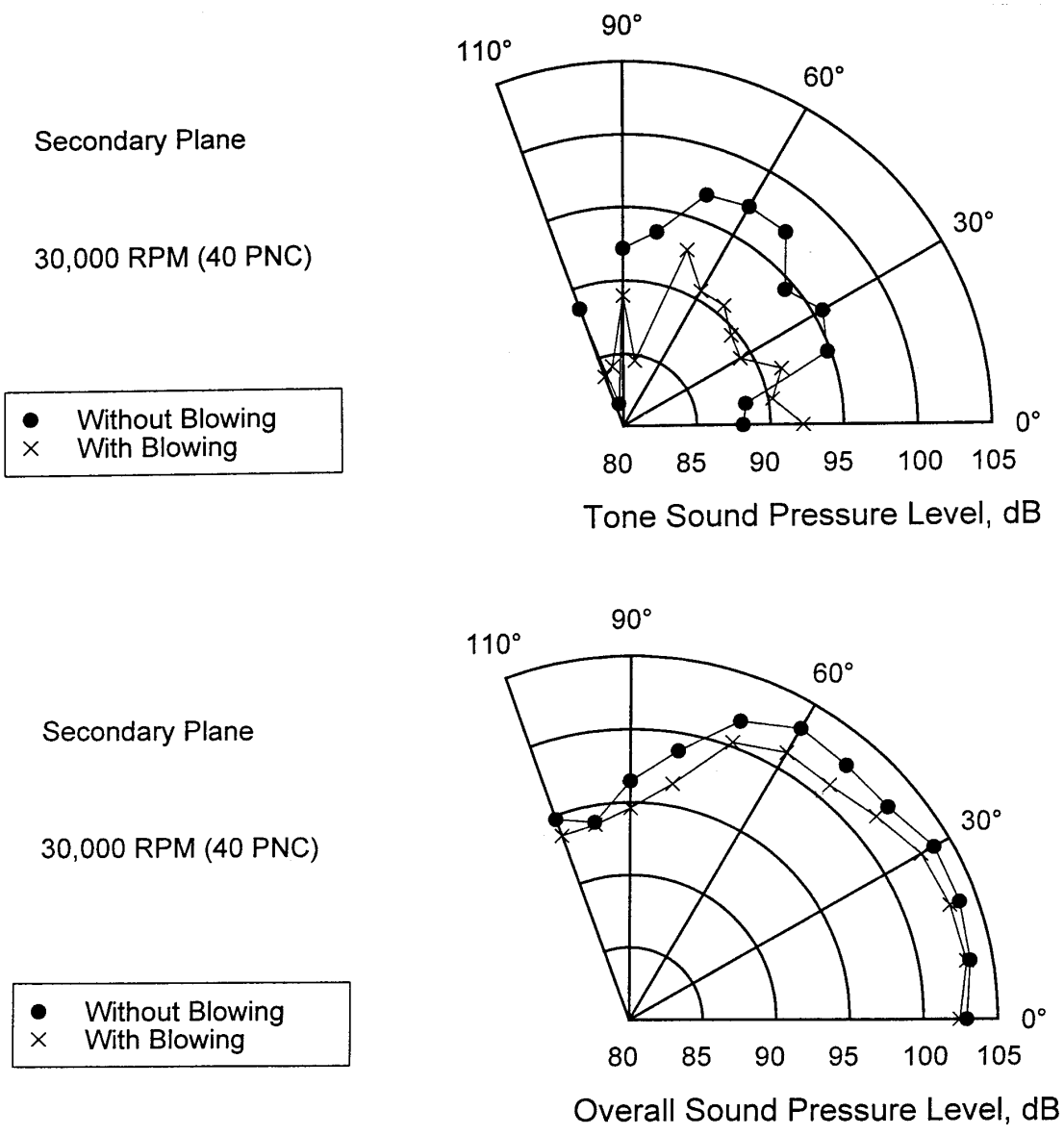

Figure 4.12 Directivity Plots at 40 PNC, Secondary Plane

Figure 4.13 shows the effect of trailing edge blowing from the stators on the tone and overall sound pressure levels for the primary plane at 50,000 RPM (60 PNC). These values are shown in Tables 4.7 and 4.8. The maximum reduction in the tone SPL was 5.5 dB at 110°, while the average reduction from 0° to 110° was 2.6 dB. The overall SPL was reduced by 0.5 dB at each location.

Table 4.7 Tone SPL for the Primary Plane at 50,000 RPM (60 PNC)

Microphone Position	Tone SPL (dB) Without Blowing	Tone SPL (dB) With Blowing	SPL Reduction (dB) Without - With Blowing
0°	101.5	97.4	4.0
10°	106.1	104.9	1.1
20°	103.6	99.4	4.2
30°	107.2	106.0	1.2
40°	107.7	105.3	2.4
50°	103.5	101.8	1.6
60°	103.7	101.9	1.8
70°	102.3	99.2	3.1
80°	96.6	98.3	-1.7
90°	92.7	90.6	2.1
100°	98.3	96.9	1.4
110°	96.5	91.0	5.5

Table 4.8 Overall SPL for the Primary Plane at 50,000 RPM (60 PNC)

Microphone Position	Overall SPL (dB) Without Blowing	Overall SPL (dB) With Blowing	SPL Reduction (dB) Without - With Blowing
0°	112.2	111.3	0.9
10°	113.0	112.6	0.5
20°	112.4	111.8	0.7
30°	113.8	113.3	0.5
40°	113.8	113.0	0.8
50°	112.4	112.0	0.5
60°	111.2	110.7	0.5
70°	108.9	108.1	0.8
80°	106.1	106.1	0.0
90°	104.6	104.4	0.2
100°	105.0	104.4	0.6
110°	105.4	104.7	0.7

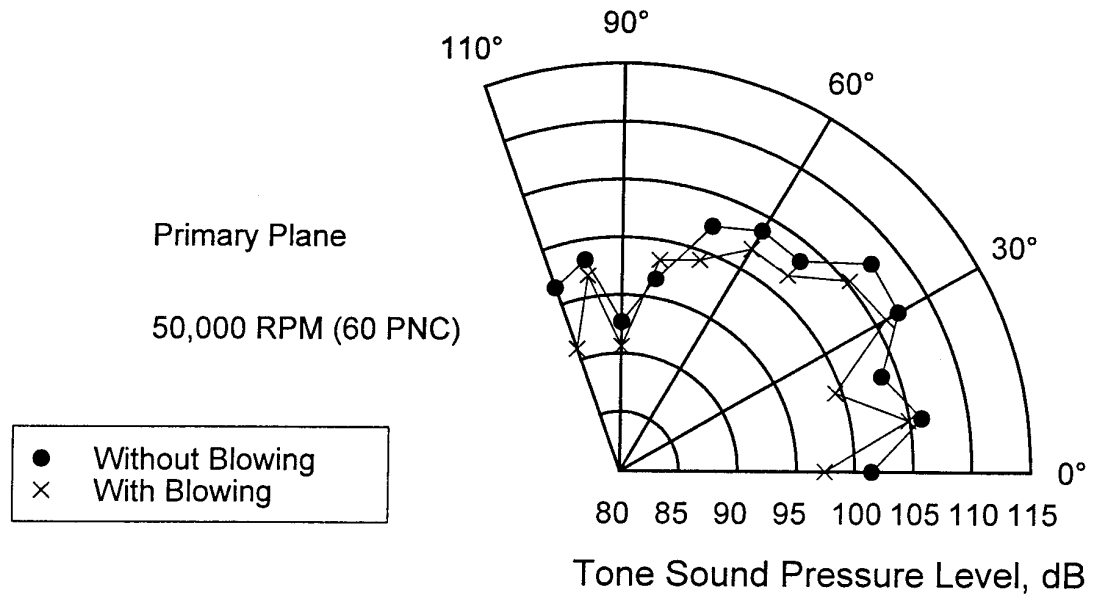

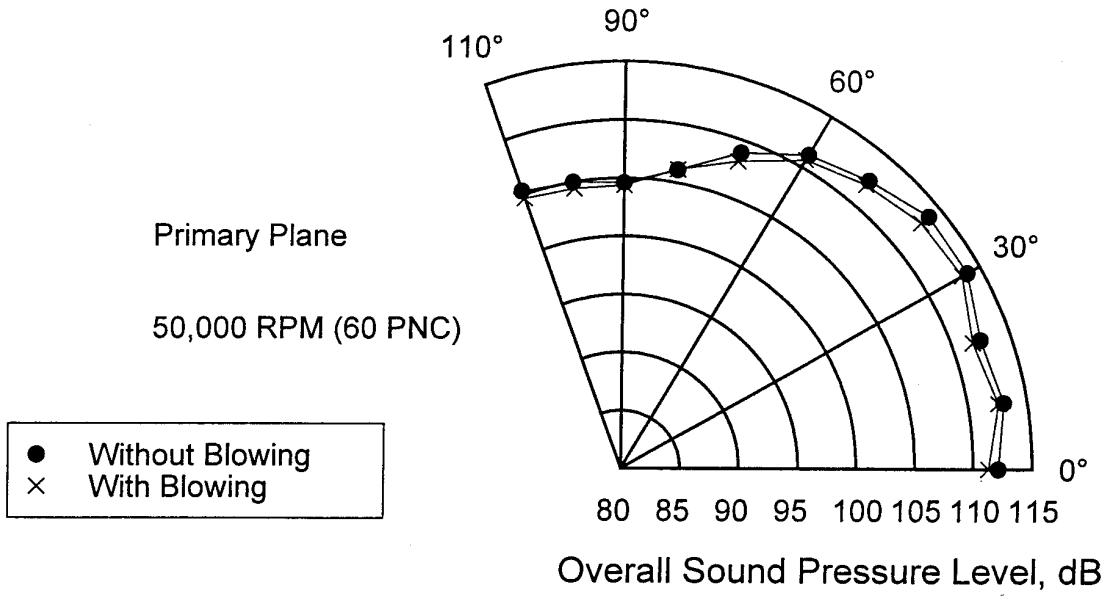

Figure 4.13 Directivity Plots at 60 PNC, Primary Plane

Figure 4.14 shows the directivity plots for the secondary plane at 50,000 RPM (60 PNC). Tables 4.9 and 4.10 show the data for these plots. The secondary plane saw a maximum reduction of 2.8 dB at 60°, and an average reduction from 0° to 110° of around 1 dB. The overall SPL was reduced by less than 1 dB at each location. Again, the overall SPL was not increased at any location.

Table 4.9 Tone SPL for the Secondary Plane at 50,000 RPM (60 PNC)

Microphone Position	Tone SPL (dB) Without Blowing	Tone SPL (dB) With Blowing	SPL Reduction (dB) Without - With Blowing
0°	105.5	106.2	-0.7
10°	100.4	99.0	1.5
20°	99.5	100.9	-1.4
30°	105.8	104.7	1.1
40°	105.8	104.7	1.1
50°	101.2	99.3	2.0
60°	106.8	104.0	2.8
70°	105.0	104.2	0.9
80°	99.2	97.9	1.3
90°	100.6	98.7	1.9
100°	94.7	94.1	0.6
110°	91.4	94.7	-3.2

Table 4.10 Overall SPL for the Secondary Plane at 50,000 RPM (60 PNC)

Microphone Position	Overall SPL (dB) Without Blowing	Overall SPL (dB) With Blowing	SPL Reduction (dB) Without - With Blowing
0°	114.5	113.9	0.6
10°	114.0	112.8	1.2
20°	113.7	113.0	0.7
30°	114.3	113.5	0.8
40°	114.3	113.8	0.5
50°	113.6	113.3	0.3
60°	113.7	113.0	0.7
70°	111.3	110.8	0.5
80°	107.7	107.0	0.7
90°	106.8	105.9	0.9
100°	105.4	104.8	0.6
110°	105.4	105.3	0.1

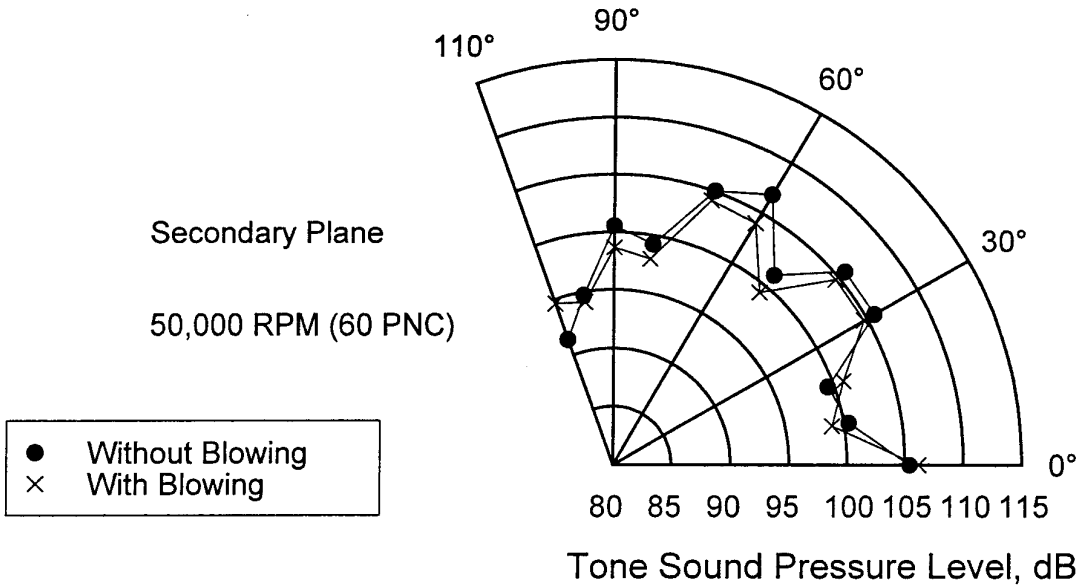

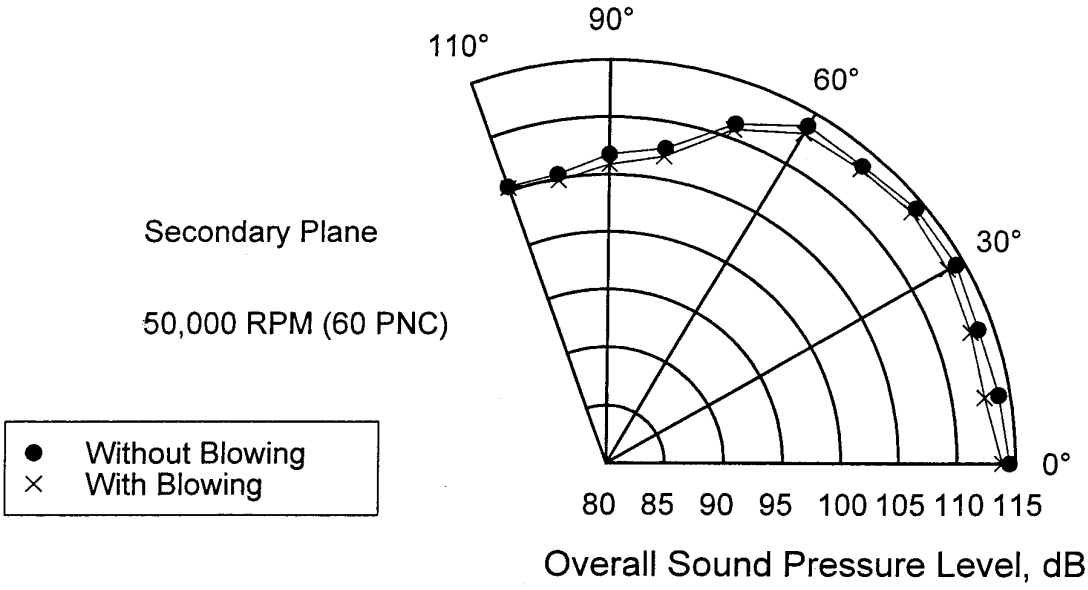

Figure 4.14 Directivity Plots at 60 PNC, Secondary Plane

Figure 4.15 shows the acoustic effects of trailing edge blowing from the stators on the primary plane at 70,000 RPM (60 PNC). The maximum reduction in the tone SPL was 2.6 dB and occured at 70°. The average reduction of the tone from 0° to 110° was 1.2 dB. The overall SPL was reduced by less than 1 dB, and was increased at only one position (50°). Tables 4.11 and 4.12 detail these figures.

Table 4.11 Tone SPL for the Primary Plane at 70,000 RPM (88 PNC)

Microphone Position	Tone SPL (dB) Without Blowing	Tone SPL (dB) With Blowing	SPL Reduction (dB) Without - With Blowing
0°	101.5	100.8	0.7
10°	101.0	97.5	3.5
20°	101.3	102.1	-0.8
30°	105.9	106.2	-0.3
40°	106.0	105.0	1.1
50°	102.4	101.4	1.0
60°	102.1	102.8	-0.8
70°	102.5	99.9	2.6
80°	102.6	100.9	1.7
90°	97.0	95.3	1.7
100°	98.3	97.8	0.5
110°	102.7	101.7	1.0

Table 4.12 Overall SPL for the Primary Plane at 70,000 RPM (88 PNC)

Microphone Position	Overall SPL (dB) Without Blowing	Overall SPL (dB) With Blowing	SPL Reduction (dB) Without - With Blowing
0°	111.6	110.6	1.0
10°	111.7	110.5	1.0
20°	112.0	110.8	1.2
30°	112.6	112.1	0.5
40°	112.6	112.4	0.2
50°	111.7	111.9	-0.2
60°	111.3	111.3	0.0
70°	110.4	109.5	0.9
80°	109.4	108.8	0.6
90°	108.4	108.1	0.3
100°	108.4	108.1	0.3
110°	109.4	109.0	0.3

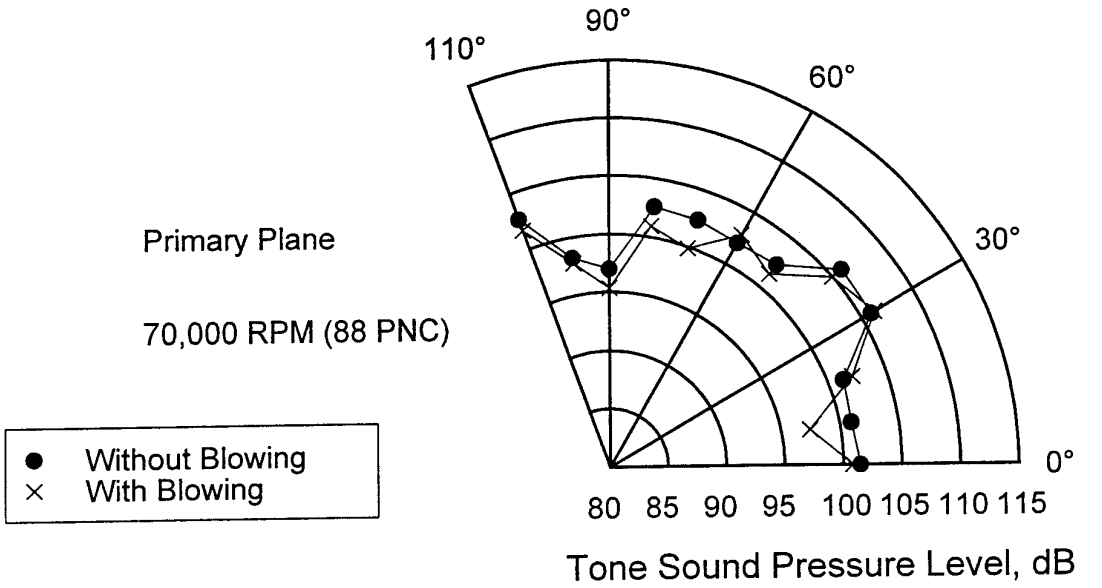

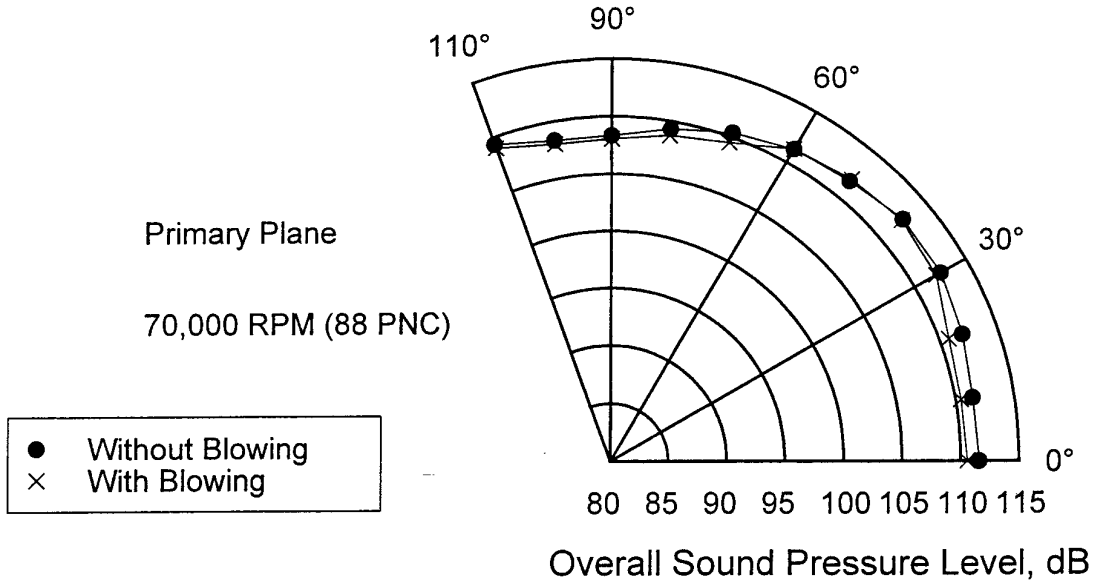

Figure 4.15 Directivity Plots at 88 PNC, Primary Plane

Although trailing edge blowing lowered the tone and overall sound pressure levels at 50,000 RPM (60 PNC) and 70,000 RPM (88 PNC), the most dramatic reductions occurred at 30,000 RPM (40 PNC). One reason that there was a larger noise reduction at 40 PNC is the flow velocity. The area-averaged fan face Mach numbers were 0.136 at 40 PNC and 0.238 at 60 PNC. Although no aerodynamic data was taken for this inlet at 88 PNC, data from a similar inlet tested by Miller (1995) shows an area-averaged fan face Mach number of 0.420. Not surprisingly, the most dramatic noise reductions due to blowing occurred at 40 PNC followed by 60 PNC and 88 PNC. Figures 4.6 and 4.7 indicate that as the wakes become deeper with higher flow velocities, it is more difficult to re-energize the wakes. The acoustic data in the previous directivity plots supports this conclusion. Even though there were notable noise reductions at each of the test speeds, trailing edge blowing had a negligible effect near the hub based on the contour plots. This indicates that the tip plays a much more significant role in noise generation than the blade span near the hub. Although there was a greater reduction in the circumferential distortion parameter at 60 PNC, there was a greater reduction in the tone SPL at 40 PNC. The distortion parameter is dominated by the fact that the stator wakes at 50,000 RPM (60 PNC) are much deeper than those at 30,000 RPM (40 PNC). Consequently, there is not a direct relationship between this distortion parameter and the tone SPL in this experiment. Note that in each case the overall SPL was reduced by trailing edge blowing. However, the broadband noise in the acoustic spectra remained unchanged. This decrease in the overall SPL is a consequence of reducing the tone SPL, and is not related to any change in the broadband noise.

4.2.3 Acoustic Repeatability

An important aspect of these measurements is the repeatability. At certain positions, the changes in SPL are relatively small. If these reductions are smaller than the variability inherent to the measurements, then it would not be appropriate to draw any conclusions from the data. For the primary plane at 30,000 RPM (40 PNC) measurements were taken from 40° to 80° on three different occasions. Ideally these numbers should have been the same, but Table 4.13 illustrates the results. The numbers in Tables 4.13 and 4.14 are the SPL reductions ($SPL\ Reduction = SPL_{without\ blowing} - SPL_{with\ blowing}$.)

Table 4.13 Acoustic Repeatability of Tone SPL at 30,000 RPM (40 PNC)

	September 1996	December 1996 (1)	December 1996 (2)	
Microphone Position	**Reduction of Tone SPL (dB)**	**Reduction of Tone SPL (dB)**	**Reduction of Tone SPL (dB)**	**Avg. Reduction of Tone SPL (dB)**
40°	1.8	2.2	4.9	3.2
50°	4.2	2.5	4.7	3.9
60°	7.2	5.4	7.0	6.6
70°	5.7	3.3	5.6	5.0
80°	6.7	8.8	11.6	9.5

Table 4.14 Acoustic Repeatability of Overall SPL at 30,000 RPM (40 PNC)

	September 1996	December 1996 (1)	December 1996 (2)	
Microphone Position	**Reduction of Overall SPL (dB)**	**Reduction of Overall SPL (dB)**	**Reduction of Overall SPL (dB)**	**Avg. Reduction of Overall SPL (dB)**
40°	0.6	0.5	0.5	0.6
50°	0.8	0.5	1.1	0.8
60°	1.2	0.9	1.7	1.3
70°	0.9	0.5	0.1	0.5
80°	1.2	1.2	1.8	1.4

In both cases, the discrepancies between the measurements are relatively small. Note that the overall SPL is much more steady than the tone. This variability in the SPL reductions was small enough that the reductions measured in these experiments were outside of the normal variability of the acoustic measurements.

4.2.4 Modal Analysis

The generation, transmission, and radiation of acoustic modes in the simulator was discussed in Chapter 2.2. Tables 4.15, 4.16, and 4.17 detail the predicted acoustic performance of the inlet used in these experiments. These tables include the radial modes up through $m = 1$ which propagate into the far field. The lower order radial modes are of particular interest because the higher radial modes either do not propagate or begin to propagate (cut on) at successively higher speeds that the $m = 0$ mode. Recall that *m* denotes the circumferential order of the mode, and m is the number of nodes or zero-pressure points across the radius of the inlet. In the

following tables the interaction between the rotors and the 26 downstream stators is denoted as (simulator), while the interaction between the rotor and the 4 upstream stators is denoted as (inlet).

Table 4.15 Acoustic Predictions at 30,000 RPM (40 PNC)

Interaction	Mode (m,n)	Cut-Off Frequency	Cut-On	Primary Lobe Radiation Angle
Rotor-Stator (simulator)	(8,0)	10060 Hz	No	Doesn't Radiate
Rotor- Stator (inlet)	(2,0)	2980 Hz	Yes	19.3°
Rotor- Stator (inlet)	(2,1)	6727 Hz	Yes	48.4°
Rotor- Stator (inlet)	(6,0)	7860 Hz	Yes	60.8°

Table 4.16 Acoustic Predictions at 50,000 RPM (60 PNC)

Interaction	Mode (m,n)	Cut-Off Frequency	Cut-On	Primary Lobe Radiation Angle
Rotor-Stator (simulator)	(8,0)	10060 Hz	Yes	42.1°
Rotor-Stator (simulator)	(8,1)	14757 Hz	Yes	79.7°
Rotor- Stator (inlet)	(2,0)	2980 Hz	Yes	11.5°
Rotor- Stator (inlet)	(2,1)	6727 Hz	Yes	26.6°
Rotor- Stator (inlet)	(2,2)	11591 Hz	Yes	50.6°

Table 4.17 Acoustic Predictions at 70,000 RPM (88 PNC)

Interaction	Mode (m,m)	Cut-Off Frequency	Cut-On	Primary Lobe Radiation Angle
Rotor-Stator (simulator)	(8,0)	10060 Hz	Yes	28.6°
Rotor-Stator (simulator)	(8,1)	14757 Hz	Yes	44.6°
Rotor-Stator (simulator)	(10,0)	12283 Hz	Yes	35.8°
Rotor-Stator (simulator)	(10,1)	17238 Hz	Yes	55.2°
Rotor- Stator (inlet)	(2,0)	2980 Hz	Yes	8.2°
Rotor- Stator (inlet)	(2,1)	6727 Hz	Yes	18.7°
Rotor- Stator (inlet)	(6,0)	7860 Hz	Yes	22.0°
Rotor- Stator (inlet)	(6,1)	12103 Hz	Yes	35.2°
Rotor- Stator (inlet)	(10,0)	12283 Hz	Yes	35.8°
Rotor- Stator (inlet)	(10,1)	17238 Hz	Yes	55.2°

In order for a mode to propagate in the inlet, its frequency must be above the cut-on frequency for that particular mode. At 30,000 RPM (40 PNC) the BPF is 9,000 Hz, which is below the cut-off frequency for the (8,0) mode produced by rotor-stator (simulator) interaction. Therefore, the only modes which should propagate to the far field at 30,000 RPM (40 PNC) are due to the rotor-stator (inlet) interaction. Since these experiments involved reducing rotor-stator (inlet) noise, the test speed of 30,000 RPM (40 PNC) is of particular interest. The radiation pattern of the blade passing tone at 40 PNC is somewhat unique. Unlike 50,000 RPM (60 PNC) and 70,000 RPM (88 PNC), there are clear lobes where the SPL reduction is quite significant (particularly between 30° and 90°). Looking at the modal analysis, there are major lobes predicted at 19°, 48°, and 61°. Not surprisingly, this speed showed the greatest noise reduction from trailing edge blowing.

The predicted positions for the primary lobes of each of the radiated patterns correspond fairly well with the analytical results, especially for many of the m= 0 modes and lower order circumferential modes. However, there are several predicted lobes that did not show up in the experimental data. For example, there was no lobe near the 80° position at 50,000 RPM (60 PNC). Likewise, there was no lobe at the 55° position at 70,000 RPM (88 PNC). Tyler and Sofrin (1962) describe a discrepancy between analytical and experimental results near the sideline region for modes that are only slightly above the cut-off frequency. The modes mentioned above

at 50,000 RPM (60 PNC) and 70,000 RPM (88 PNC) were relatively near their respective cut-off frequencies. This departure could be due to the assumption in the radiation analysis that the particle velocity at the duct exit is assumed to be zero.

5.0 Conclusions

This study is a preliminary step toward investigating the aeroacoustic effects of blowing from the trailing edges of stators in an aircraft engine inlet. A reduced number of stators (4) was tested in a 1/14 scale model inlet with a 4.1 in (10.4 cm) diameter turbofan engine simulator. These tests were performed at three different simulator fan speeds: 30,000 RPM (40 PNC), 50,000 RPM (60 PNC), and 70,000 RPM (88 PNC). The test speed of 60 PNC corresponds to aircraft approach conditions, while 88 PNC simulates takeoff conditions. The results show notable reductions of the tone SPL at all test speeds. In addition, the overall sound pressure level was reduced at nearly all measurement locations.

An important part of this investigation was designing the trailing edge configuration of the stators to accomplish the blowing. It is unlikely that the hole size and distribution from these experiments could be scaled or extrapolated and successfully used in another application. The most appropriate trailing edge configuration will vary from one application to another, depending upon the geometry and specifications.

The aerodynamic results indicate the ability to re-energize the wakes near the mid span and tip sections of the upstream stators. In doing so, the circumferential distortion is clearly reduced. At the higher speeds, the wakes are deeper with higher velocity flows. These factors combine to make it more difficult to re-energize the wakes a higher speeds.

The acoustic spectra indicate that trailing edge blowing is capable of significant reductions of the tone SPL at each of the test speeds. At the same time, there was no significant change in the broadband noise. At 70,000 RPM (88 PNC), the trailing edge blowing was successful in reducing some of the multiple pure tones. It is believed that as a consequence of the shocks' highly nonlinear nature, the amplitude and spacing differences made the combination tones difficult to control.

The most dramatic noise reductions were recorded at 30,000 RPM (40 PNC). The results at this speed are of particular interest because the interaction between the rotors and the stators in the simulator was cut-off, leaving only the rotor-stator interaction in the inlet. There was a

maximum reduction of 8.9 dB in the tone, and an average reduction of 6.2 dB between the 30° and 90° microphone locations. The overall SPL was reduced by approximately 1 dB at each microphone position, and was not increased at any measurement location by the trailing edge blowing.

While the tone reductions at 30,000 RPM (40 PNC) were particularly significant between the 30° and 60° microphone locations, the tone at 50,000 RPM (60 PNC) was reduced by an average of 2.6 dB from 0° to 110°. The maximum reduction in the tone SPL was 5.5 dB. Again, the overall SPL was consistently reduced by approximately 1 dB at each microphone location.

The noise reductions at 70,000 RPM (88 PNC) were not as dramatic as those at 50,000 RPM (60 PNC) and 30,000 RPM (40 PNC). The maximum reduction in the tone SPL at 70,000 RPM (88 PNC) was 2.6 dB, while the overall SPL was reduced by less than 1 dB from 0° to 110°. These acoustic results substantiate the aerodynamic data which indicates difficulty in re-energizing wakes in higher speed flows.

One reason that 30,000 RPM (40 PNC) showed the greatest noise reduction due to blowing was that the interaction between the rotors and stators in the simulator was cut-off. Unlike the other speeds, the only modes which propagated at 40 PNC were the ones which had been effected by trailing edge blowing from the four upstream stators. Another reason for the reduction at 40 PNC is the lower flow velocity. The area-averaged Mach number at the fan face was 0.136, 0.239, and approximately 0.4 for 40 PNC, 60 PNC, and 88 PNC, respectively. As the wakes become deeper in the higher velocity flows, it is more difficult for the trailing edge blowing to manage the unsteady rotor-stator interaction and prevent noise radiation.

The addition of trailing edge blowing did not change the operating point of the fan at either speed. The total pressure ratio with and without blowing was 1.07 at 30,000 RPM (40 PNC) and 1.18 at 50,000 RPM (60 PNC). The amount of air added by the trailing edge blowing was small in comparison to the overall flow through the fan at all test speeds.

The results of this investigation clearly demonstrate that trailing edge blowing from the stators is effective in reducing unsteady rotor-stator interaction and the subsequent forward radiated noise. Most importantly, these results encourage a more in depth investigation using an increased stator count in the inlet.

It is apparent that experiments in a small-scale test program provide a low cost alternative to develop a better understanding of aircraft engine acoustics. Future aeroacoustics work can focus on several areas. Having shown trailing edge blowing to be effective with the four upstream stators in these experiments, the next step is to use trailing edge blowing with an increased stator count. Ultimately, the trailing edge blowing could be extended to the rotating fan blades in the engine. However, there are a number of issues to be addressed. Since rotors and stators in an actual engine are very closely spaced, an important consideration is how the effectiveness of trailing edge blowing varies with axial distance. For trailing edge blowing to be

feasible in a full-scale engine, the performance at high speeds must be enhanced to give greater noise reductions. It is reasonable to expect that any improvement in the wake mixing would result in a reduction in the radiated noise. These experiments showed significant noise reductions without re-energizing the wakes near the hub sections. Perhaps a blowing profile could be designed that would target distortion near the mid span and tip regions of the fan. In this way, a lower mass flow of blowing air could be used to achieve a noise reduction. In addition to aeroacoustics, trailing edge blowing could have applications in areas such as high cycle fatigue in the blades. By eliminating the wakes from upstream stators, the unsteady loading on the blades could be reduced. It is this periodic loading and unloading with each shaft rotation that results in fatigue failure in the rotor blades.

Appendix A Bench Test

The purpose of this bench test was to determine the optimum hole configuration at the trailing edges of each of the four blowing stators used in the inlet. The different hole configurations were evaluated based only on aerodynamic measurements of static and total pressure in the stator wake, no acoustic measurements were made on the bench test. These measurements were examined to identify which hole configuration provided to most uniform blowing profile from tip to hub. Once a desirable trailing edge configuration was found, four stators were manufactured to be used in the actual inlet. The bench test was then used to prove that all four stators did, in fact, perform similarly.

The bench test setup consisted of a test stator fixed between two pieces of Plexiglas as shown in Figure A.1. Blowing air was supplied from the plenum to the test stator through the top piece of Plexiglas. To simulate how the blowing stator would behave with air flowing past the stator, the entire setup was immersed in air flow from a high-speed blower. The blowing configuration was identical to that used in the actual inlet. The same copper tubing was used to pipe air from the air cylinder to the plenum and then to the stator.

The goal in designing the trailing edge configuration was to produce a uniform blowing profile at the trailing edge of the stator while minimizing the mass flow used. The main problem is that the only exit from the circular passage is through the trailing edge blowing holes. The flow reaches the bottom of the passage and stagnates, causing a rise in total pressure. Because of this non-uniform pressure profile inside the supply passage, it is difficult to achieve a uniform blowing profile at the trailing edge. If equally-spaced holes of the same diameter are used, most of the blowing air exits through the bottom holes. This problem could have been solved in one of two ways: by tapering the air supply passage that feeds the trailing edge holes, or by making the trailing edge holes at the hub larger than the holes at the tip. For manufacturing purposes, the simplest solution was to use larger holes at the tip and smaller holes at the hub.

Two configurations were tested: six equally spaced holes and nine equally spaced holes. Each of the holes were drilled to a diameter of 1/16 in. In order to experiment with different hole

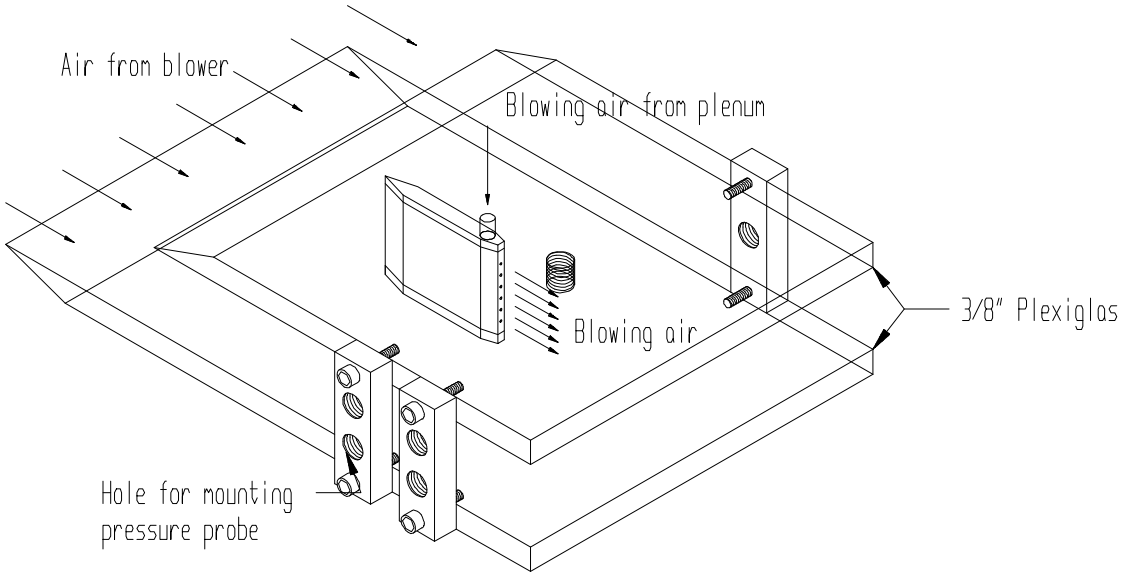

Figure A.1 Bench Test Apparatus

sizes, different pieces of 1/16 in OD steel tubing were inserted into the holes. Using pieces of steel tubing with different inner diameters made it possible to test a particular configuration of holes, replace the inserts with different inner diameters, and then test another configuration. Using these inserts, only two test struts were needed to experiment with a variety of trailing edge configurations. The drawback to using these inserts to vary the inner diameters of the steel inserts are only made in standard increments. Therefore, the hole sizes are limited by the availability of steel inserts. After extensive testing, it was found that six equally-spaced holes provided the best results in neutralizing the wake. In addition, six holes used less blowing air.

Two types of aerodynamic measurements were made on the stator wakes, radial measurements from tip to hub and measurements perpendicular to the stators. The radial traverses were at a downstream distance of 25% of the stator chord length from the trailing edge. The traverses perpendicular to the stator were at a downstream distance of 50% of the stator chord length from the trailing edge. Three perpendicular traverses (equally-spaced from tip to hub) were made. Each of these measurements was made using the same Pitot-static probe that was later used in the anechoic chamber experiments. It was very important to identify how the stator was performing all along its span from tip to hub. There were cases where a particular hole configuration effectively neutralized the wake at the hub and midspan, but performed very poorly at the tip. Figures A.2 and A.3 show the aerodynamic results from this stator. Obviously, it was not possible to produce a perfectly uniform profile; however, this configuration performed the best.

Once the trailing edge configuration had been found, four stators to be used in the actual inlet were manufactured according to the specifications. The bench test was next used to make sure that each of the inlet stators performed just as the test stator had. In addition, it was important to make certain that each of the four inlet stators performed the similarly. Figure A.4 compares the performance of all four inlet stators based on radial traverses from the tip to hub without the high-speed blower running. This figure clearly shows that the blowing profile is relatively uniform from tip to hub and that all of the stators perform very similarly. In addition to the above mentioned data, the bench test provided an excellent opportunity to test various aspects of the experimental setup. For example, the effects of bending the air supply lines to each of the stators were examined to determine how these additional losses effect the trailing edge blowing and wake management performance.

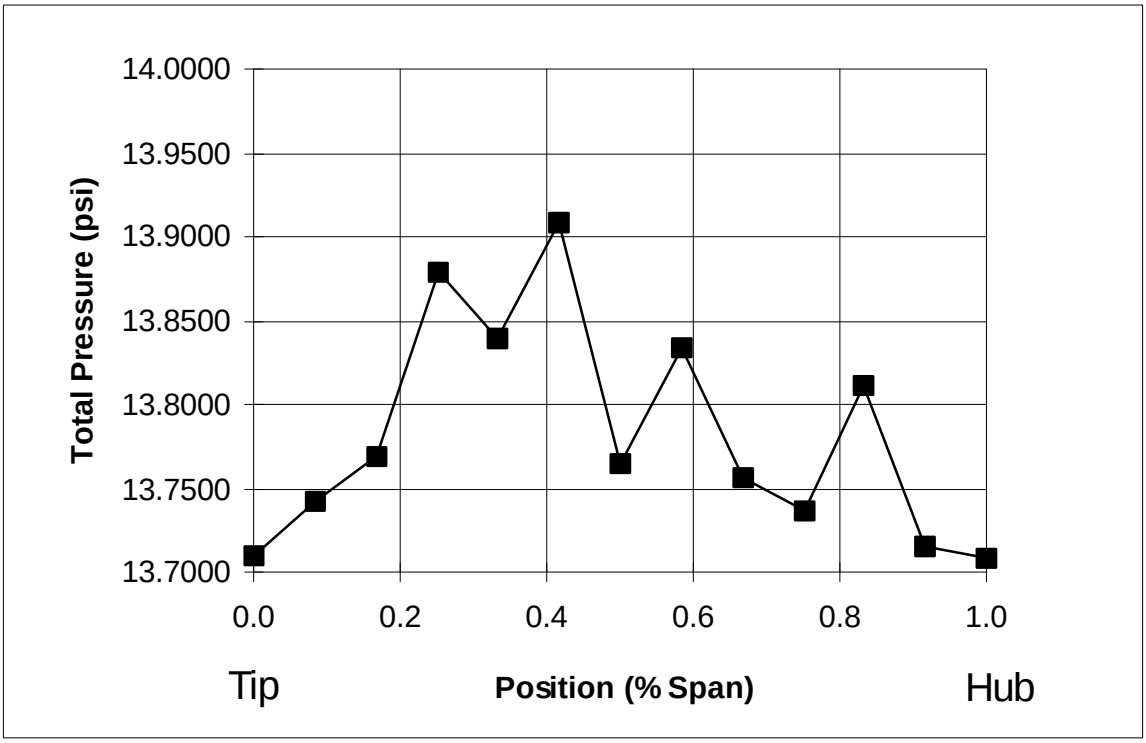

Figure A.2 Results for the Test Stator (Radial Traverse)

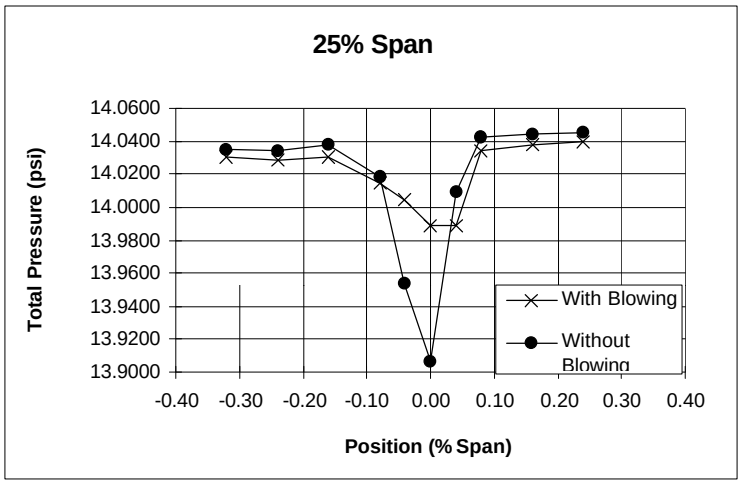

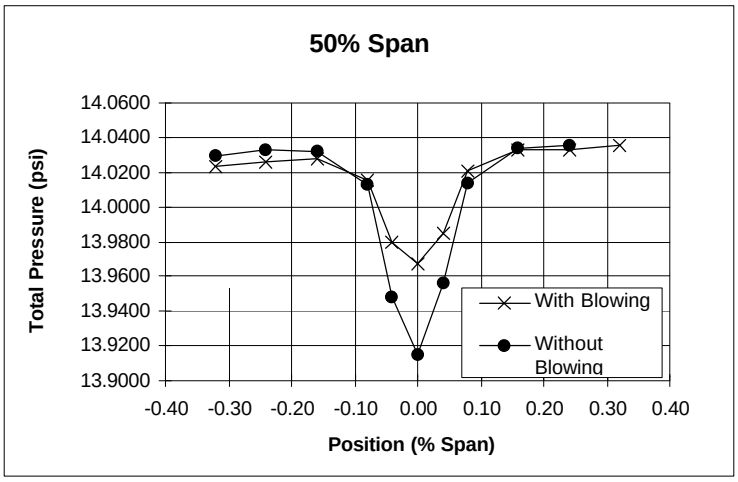

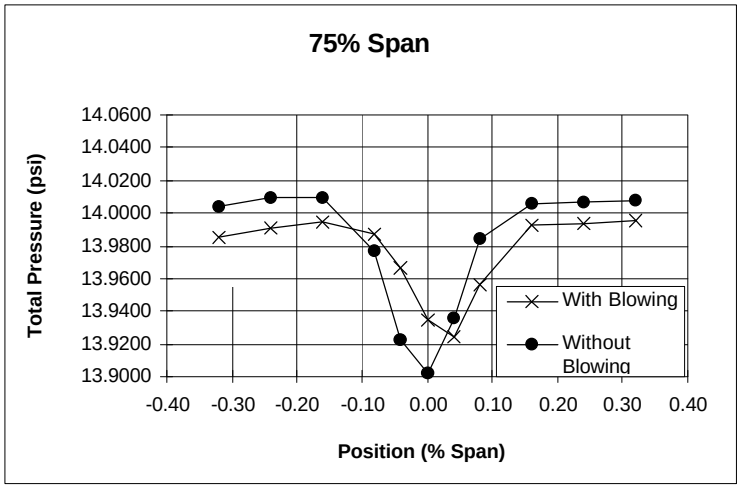

Figure A.3 Results for the Test Stator

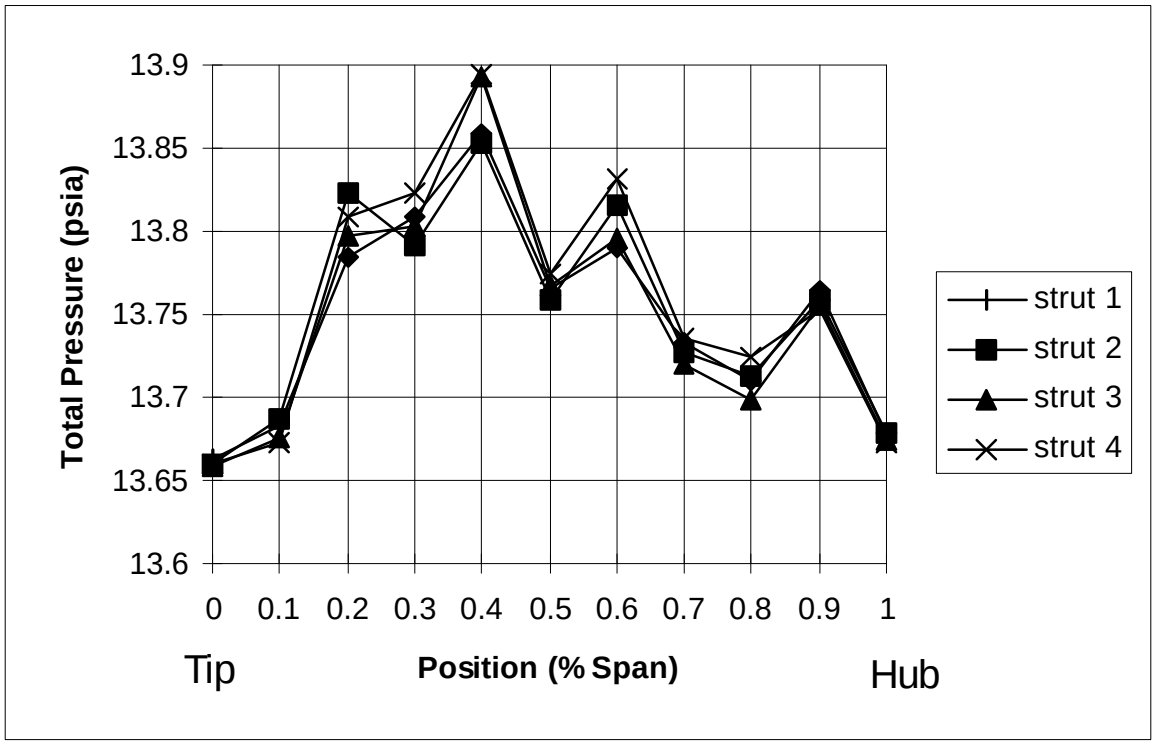

Figure A.4 Discrepancies Between the Inlet Stators (Radial Traverses)

Appendix B Sensitivity to Blowing Rate

The acoustic results in these experiments were very sensitive to the blowing rate. It is clear that using trailing edge blowing can either decrease or increase the radiated noise. The first step in the acoustic testing was to determine which blowing rate to use at each speed. One microphone was placed at the 20° position and one microphone was placed at the 80° position. The tone and overall sound pressure levels were measured first without blowing and then with several different blowing rates in the primary plane. The blowing rate was incremented until a maximum SPL reduction was achieved. Figures B.1 through B.3 show how the noise reduction varied with blowing rates for the three test speeds (40 PNC, 60 PNC, and 88 PNC). Note that the blowing rate was controlled by varying the upstream pressure in the plenum. The blowing rates in Figures B.1 through B.3 are plotted in terms of this upstream pressure. The blowing rates chosen for each speed are shown in Table B.1. In each of these figures the noise reductions is defined as $dB\ Reduction = SPL_{without\ blowing} - SPL_{with\ blowing}$.

Table B.1 Optimum Blowing Rate

Simulator Test Speed	Optimum Plenum Pressure
30,000 RPM (40 PNC)	20 psia
50,000 RPM (60 PNC)	25 psia
70,000 RPM (88 PNC)	32 psia

There was no formula used to evaluate the best blowing rate for each speed. The optimum blowing rate was chosen by examining what upstream pressure resulted in the largest reductions in the tone SPL and overall SPL at the 20° and 80° positions. The best blowing rate was chosen based only on the data shown in Figures B.1 through B.3. These decisions were somewhat subjective. At each position the optimum blowing rate to reduce the tone SPL was clear, with noise reduction falling off somewhat rapidly above and below the optimum pressure. However, at each of the speeds the best blowing rate was different for the 20° position and the

80° position. Clearly, each angular position in the radiation pattern is effected somewhat differently by different blowing rates.

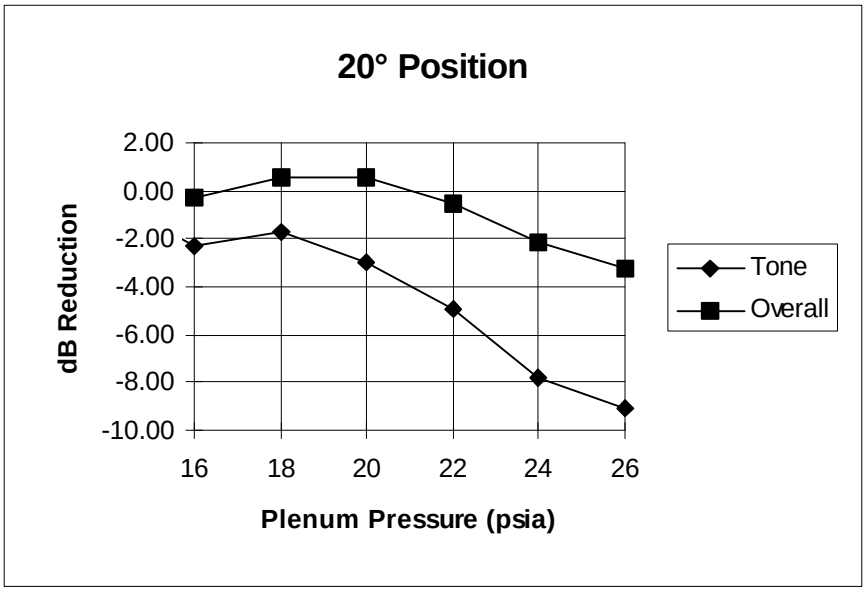

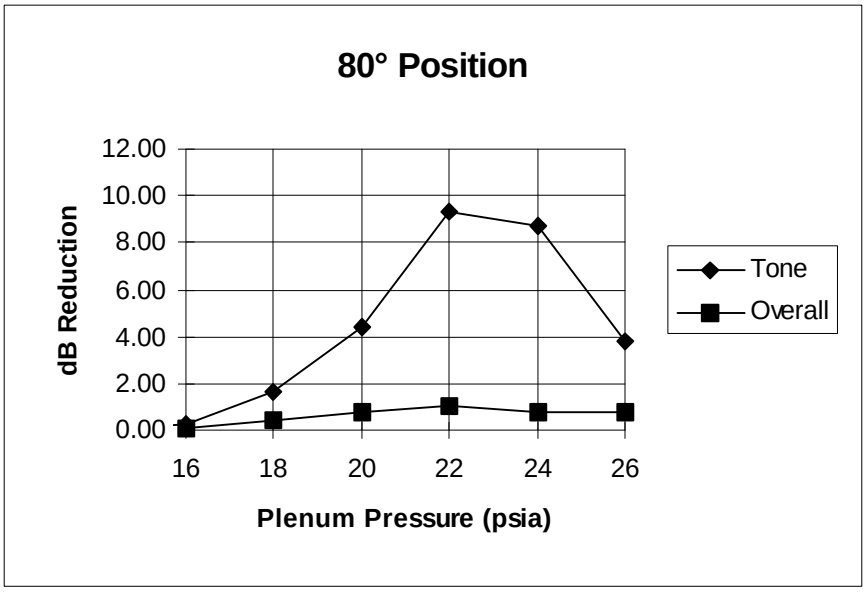

Figure B.1 Acoustic Sensitivity to Blowing Rate, 40 PNC

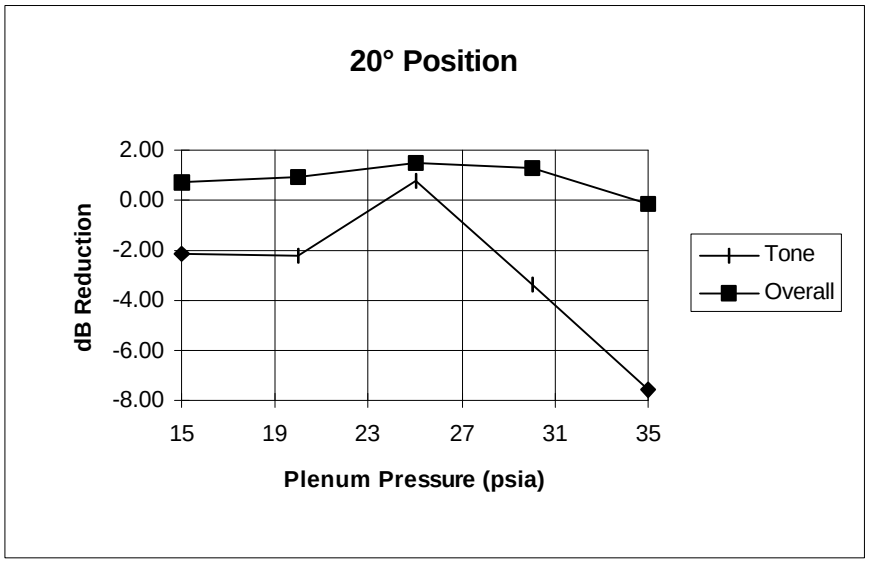

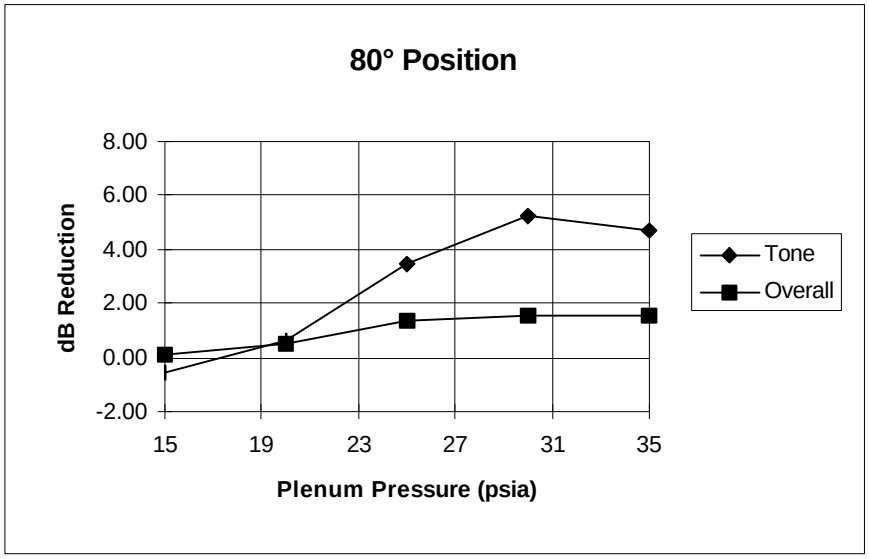

Figure B.2 Acoustic Sensitivity to Blowing Rate, 60 PNC

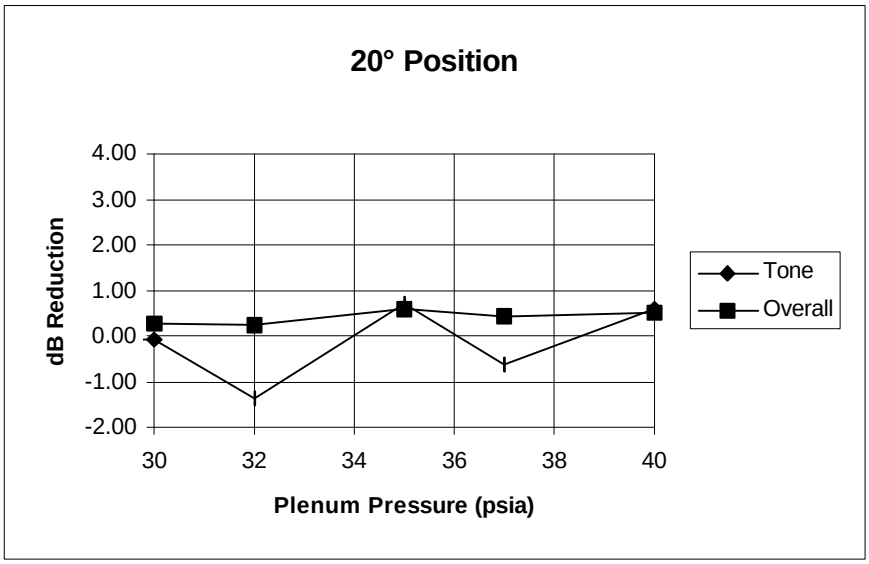

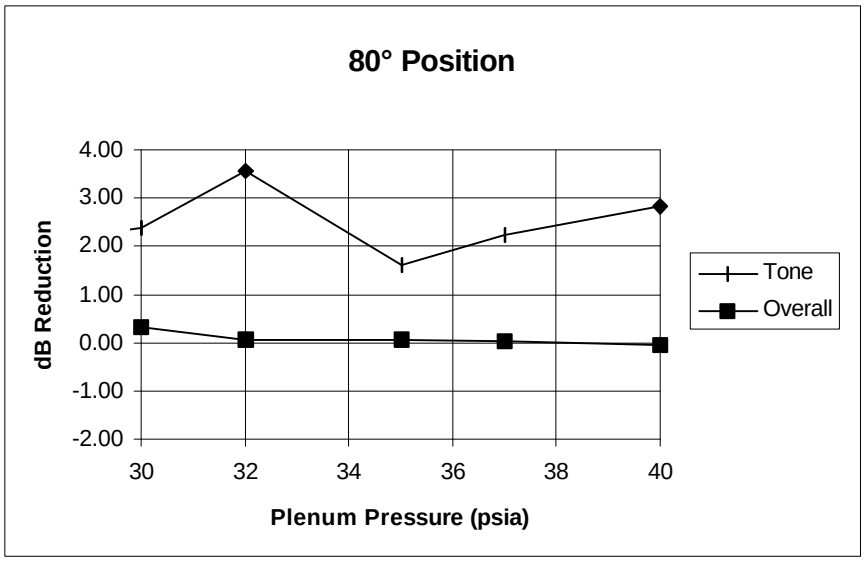

Figure B.3 Acoustic Sensitivity to Blowing Rate, 88 PNC

References

Corcoran, Timothy, "Control of the Wake from a Simulated Blade by Trailing Edge Blowing," Masters Thesis, Mechanical Engineering Department, Lehigh University, 1992.

Cumpsty, N.A. Compressor Aerodynamics. New York: John Wiley & Sons, 1989.

Detwiler, K.P. "Reduced Fan Noise Radiation from a Supersonic Inlet," Masters Thesis, Mechanical Engineering Department, Virginia Polytechnic Institute & State University, Blacksburg, Virginia, April 1993.

Hale, J.H. "Effects of Stationary Wake on Turbine Blade Heat Transfer in a Transonic Cascade," Masters Thesis, Mechanical Engineering Department, Virginia Polytechnic Institute & State University, Blacksburg, Virginia, April 1996.

Kerrebrock, Jack L. Aircraft Engines and Gas Turbines. Cambridge, Massachusetts: The MIT Press, 1978.

Kinsler, L.E., Frey, A.R, Coppens, A.B., and Sanders, J.V. Fundamentals of Acoustics. 3rd ed. New York: John Wiley & Sons, 1982.

Model 460 Turbofan Propulsion Simulator Products Specification, Tech Development Inc., U.S. Patent 3434679.

Naumann, R. Georg, "Control of the Wake from a Simulated Blade by Trailing Edge Blowing," Masters Thesis, Mechanical Engineering Department, Lehigh University, 1992.

Nuckolls, W.E. and Ng, W.F., "Fan Noise Reduction from a Supersonic Inlet During Simulated Aircraft Approach." ASME 93-GT-279, May 1993.

Pande, A., Ng, W. F., "Effects of Struts on the Aeroacoustics of Axisymmetric Supersonic Inlets," Masters Thesis, Mechanical Engineering Department, Virginia Polytechnic Institute and State University, November 1994.

Park, W.J., and Cimbala, J.M., "The Effects of Jet Injection Geometry on Two-dimensional Momentumless Wakes," Journal of Fluid Mechanics, Vol. 224, pp. 29-47, 1991.

Saunders, J.D., Keith, T.G., "Results from Computational Analysis of a Mixed Compression Supersonic Inlet," AIAA 91-2581, June 1991.

Seddon, J. and E.L. Goldsmith. Intake Aerodynamics. Ed. J.S. Przemieniecki. New York: AIAA, 1985.

Succi, G.P., "System and Method for Suppression Noise Produced by Rotors," United States Patent No. 5217349, 1993.

Trefney, C.J., Wasserbauer, J.W. "Low-Speed Performance of an Axisymmetric, Mixed-Compression, Supersonic Inlet with Auxiliary Inlets," NASA TP-2557, February 1986.

Tyler, J. M., and Sofrin, T.G., "Axial Compressor Noise Studies," SAE Transactions, Vol. 70, 1962.

Wagner, R. "Aeroacoustics of the Bifurcated 2D Supersonic Inlet," Masters Thesis, Mechanical Engineering Department, Virginia Polytechnic Institute & State University, Blacksburg, Virginia, December 1994.

Waitz, I.A., Brookfield, J.M., Sell, J., and Hayden, B.J., "Preliminary Assessment of Wake Management Strategies for Reduction of Turbomachinery Fan Noise," First Joint CEAS/AIAA Aeroacoustics Conference, Munich, Germany, 1995.

Vita

Thomas Leitch was born in Covington, Virginia on January 9, 1972, and graduated from Covington High School. He graduated *Summa Cum Laude* from Virginia Polytechnic Institute & State University in 1995 with a Bachelor of Science in Mechanical Engineering, and immediately began his graduate studies at Virginia Tech working for Dr. W.F. Ng. The author defended his work on January 16, 1997.

_____

Thomas A. Leitch